Université de Montréal

USING BIOID TO STUDY RAS SIGNALING TO THE HIPPO PATHWAY

Par Maya Nikolova

Programmes de biologie moléculaire
Faculté de Médecine

Mémoire présenté en vue de l'obtention du grade de M.Sc. en biologie moléculaire option générale

Août 2022

Résumé

RAS est une GTPase qui transduit les signaux extracellulaires envers des voies de signalisation intracellulaires, en liant ses effecteurs. RAS peut activer la voie Hippo qui inhibe la croissance cellulaire et qui est souvent dérégulée dans le cancer. Les protéines RASSF suppresseurs de tumeurs relient RAS à la voie Hippo. L'expression exogène de $KRAS^{G12V}$ avec RASSF1 ou RASSF5 conduit à l'activation de la voie Hippo, bien que KRAS et RASSF1 ne s'associent pas directement.

Ce projet de maîtrise vise à identifier les protéines impliquées dans l'activation de la voie Hippo par RAS. Nous avons effectué plusieurs expériences BioID, une technique qui permet d'identifier les interacteurs proximaux d'une protéine d'intérêt, dans des lignées cellulaires U2OS stables et inductibles exprimant les protéines $KRAS^{G12V}$, RASSF1 ou RASSF5 seules ou coexprimées, permettant de comparer les conditions où la voie Hippo inactive ou active. Nous avons élucidé l'interactome d'un mutant de KRAS avec affinité accrue envers RASSF5 et affinité réduite envers RAF, permettant d'étudier les voies activées en aval de RASSF5, avec une activation réduite de la voie MAPK. Nos données montrent que RASSF1 et RASSF5 relâchent les kinases Hippo MST1 et MST2 lorsque la voie Hippo est active, conformément aux données *in vitro* démontrant un rôle inhibiteur de l'interaction RASSF/MST. De plus, nous avons démontré que KRAS est un interacteur proximal des protéines VAMP3 et SNAP23.

Comprendre comment l'oncoprotéine RAS active des effecteurs et des voies de signalisation moins étudiés, en particulier ceux qui ont des fonctions suppressives de tumeurs a des implications importantes pour le développement de nouvelles thérapies ciblées pour les cancers induits par RAS.

Mots-clés : RAS, voie Hippo, RASSF1, RASSF5, MST, SNARE, BioID

Abstract

RAS is a small GTPase that transduces signals from membrane-bound receptors to intracellular pathways, by signaling to downstream effector proteins. RAS can activate the Hippo pathway, a growth-suppressive pathway that is often dysregulated in cancer. The tumor suppressor RASSF proteins link RAS to Hippo signaling. Co-expression of $KRAS^{G12V}$ with either RASSF1 or RASSF5 leads to Hippo pathway activation, despite KRAS and RASSF1 not being direct binding partners.

This M.Sc. project aims to identify proteins that are involved in RAS-mediated activation of the Hippo pathway. We performed BioID, a proteomic technique which is used to identify the proximal interactors of a protein of interest, in stable and inducible U2OS osteosarcoma lines expressing $KRAS^{G12V}$, RASSF1, or RASSF5 proteins alone, as well as in lines co-expressing both $KRAS^{G12V}$ and the RASSF proteins, allowing for a comparison between inactive and active Hippo pathway interactomes. Furthermore, we mapped the interactome of a double mutant of KRAS that displays increased affinity for RASSF5 and decreased affinity for the effector RAF, allowing us to study KRAS signaling downstream of RASSF5, with decreased activation of the MAPK pathway. Our BioID data shows that RASSF1 and RASSF5 disengage the Hippo kinases MST1 and MST2 when the Hippo pathway is active, in line with the inhibitory role of the RASSF/MST interaction observed *in vitro*. Furthermore, we show that KRAS is a proximal interactor of the SNARE proteins VAMP3 and SNAP23.

Understanding how the oncoprotein RAS signals to less studied effectors and pathways, particularly those with tumor suppressive functions has significant implications for understanding oncogenesis, and for development of new targeted therapies for RAS-driven cancers.

Keywords: RAS GTPase, Hippo pathway, RASSF1, RASSF5, MST, SNARE, BioID

Table of Contents

List of Tables

List of Figures

List of Abbreviations

ABC	Ammonium Bicarbonate
AFDN	Afadin
AP-MS	Affinity purification mass spectrometry
ARF	ADP-ribosylation factor
BF	Biological function
BSA	Bovine serum albumin
CC	Cellular component
CEP	Centrosomal protein
CRC	Colorectal cancer
DLG5	Discs large homolog 5
DMEM	Dulbecco's Modified Eagle Medium
DSG2	Desmoglein 2
DTT	Dithiothreitol
ECL	Enhanced Chemiluminescence
EDTA	Ethylenediaminetetraacetic Acid
EGF	Epidermal growth factor
EGTA	Ethylene glycol-bis(2-aminoethylether)-N,N,N′,N′-tetraacetic acid
EMT	Epithelial-to-mesenchymal transition
EPB41L2	Band 4.1-like protein 2
EPHA2	Ephrin type-A receptor 2
ERK	Extracellular signal-regulated kinase
FA	Formic Acid
FBS	Fetal bovine serum
FDR	False discovery rate
GAP	GTPase activating protein
GDP	Guanosine diphosphate
GEF	Guanine nucleotide exchange factor
GFP	Green fluorescent protein
GO	Gene ontology
GPCR	G-protein coupled receptor

GRB2	Growth factor receptor-bound protein 2
GST	Glutathione S-transferase
GTP	Guanosine triphosphate
HNRNPC	Heterogeneous nuclear ribonucleoproteins C1/C2
Hpo	Hippo
HRP	Horseradish peroxidase
HVR	Hypervariable region
IAP	Inhibitor of apoptosis
IGF2BP2	Insulin-like growth factor 2 mRNA-binding protein 2
IP	Immunoprecipitation
ITC	Isothermal titration calorimetry
LATS	Large tumor suppressor
LRP1	Prolow-density lipoprotein receptor-related protein 1
LUAD	Lung adenocarcinoma
MAP	Microtubule associated protein
MAPK	Mitogen-activated protein kinase
MEK	Mitogen-activated protein kinase kinase
MF	Molecular function
MOAP1	Modulator of apoptosis 1
MOB1	Mob1 homolog 1
MST	Mammalian Ste20-like kinase
NAP1L	Nucleosome assembly protein 1-like
NCKL	N149C/K208L
NCS	Newborn calf serum
NDR	Nuclear Dbf2-related kinase
NF1	Neurofibromin 1
NF2	Neurofibromin 2
NPM1	Nucleophosmin
PBS	Phosphate buffered saline
PDAC	Pancreatic ductal adenocarcinoma
PEI	Polyethyleneimine

PI3K	Phosphatidylinositol 4,5-bisphosphate 3-kinase
PIP3	Phosphatidylinositol (3,4,5)-trisphosphate
PLC	Phospholipase C
PM	Plasma membrane
PMSF	Phenylmethylsulfonyl Fluoride
RA	RAS association
RALGDS	Ral guanine nucleotide dissociation stimulator
RAS	Rat sarcoma
RASAL2	RAS protein activator-like 2
RASSF	Ras association family
RBD	RAS binding domain
RGL	Ral guanine nucleotide dissociation stimulator-like
RIN1	Ras and Rab interactor 1
RPL10	60S ribosomal protein L10
RPS3	40S ribosomal protein S3
RPS9	40S ribosomal protein S9
RTK	Receptor tyrosine kinase
SAINT	Significance Analysis of Interactome
SARAH	Salvador-RASSF-Hippo
SAV1	Protein salvador homolog 1
SCRIB	Scribble
SDS	Sodium Dodecyl Sulfate
SDS-PAGE	Sodium Dodecyl Sulfate–Polyacrylamide Gel Electrophoresis
SKA3	Spindle and kinetochore-associated protein 3
SLC3A2	Solute carrier family 3 member 2
SNAP	Synaptosomal-associated protein
SNARE	Soluble NSF attachment protein receptors
SOS1	Son of sevenless homolog 1
TAZ	Transcriptional co-activator with PDZ-binding motif
TBST	Tris buffered saline Tween-20
TCEP	Tris(2-carboxyethyl)phosphine hydrochloride

TEAD	TEA domain
TIAM1	T-lymphoma invasion and metastasis-inducing protein 1
UBE2O	E2 ubiquitin-conjugating enzyme O
VAMP	Vesicle-associated membrane protein
YAP	Yes-associated protein

Acknowledgements

There are many people who have helped and encouraged me throughout this journey. I want to begin by thanking my supervisor Dr. Matthew Smith for giving me the opportunity to work on such a fascinating project, and for supporting me every step of the way. I have truly learned a lot and grown as a scientist under his mentorship.

Thank you very much to Dr. Lea Harrington who gave me valuable feedback as my M.Sc. advisor. Special thanks to the IRIC proteomics core facility and Éric Bonneil, who performed all the mass spectrometry experiments. I would also like to thank Brett Larsen from the Lunenfeld-Tanenbaum Research Institute who patiently answered my many questions regarding BioID data analysis and the ProHits software.

I cannot thank enough everyone in the Smith lab, whose support and comradery means the world to me, and who during the long months of the pandemic were among the only people I was fortunate enough to see daily. My gratitude to all of you cannot be understated. Thank you, Dhana, for training me when I first arrived in the lab, and for trusting me with parts of your project. Thank you, Chang Hwa, for being such a positive presence in the lab. Thank you, Marilyn, for always taking time out of your day to answer my questions and to brainstorm solutions with me. Thank you, Swati, Regina, Gabriela, and Unain, for being the best lab mates and friends I could ever ask for. You girls (and our coffee breaks) are what I will remember best from my time as a M.Sc. student.

I would not have been able to accomplish any of this without my family. Thank you to my partner, Jordan, whose steady and reassuring presence is a source of joy and motivation in my life. Finally, thank you to my parents, Irina and Pirin, for teaching me to never give up on my dreams and for showing me what hard work and success looks like. Обичам ви.

INTRODUCTION

Cellular signaling pathways

Cells receive numerous signals from their environment, and they convey these signals into functional responses through signaling pathways that consist of sequential protein-protein interactions. A key feature of signaling pathways is crosstalk between pathways, as well as crosstalk between the proteins within a pathway resulting in feedforward and feedback loops and numerous branches at every node. In fact, linear signaling pathways are a way of conceptualizing the complex network of protein-protein interactions that exists within living cells, and which is extremely dynamic and responsive to external inputs (1). Modern systems biology approaches such as proteomics aim to elucidate the larger picture of cellular signal transduction networks. RAS GTPases play central roles in many signaling pathways; many of their roles in signaling are well elucidated, while others remain in the dark.

The oncoprotein RAS

RAS small GTPases

RAS is a small membrane bound GTPase that transduces signals from cell surface receptors to intracellular signaling pathways (2). RAS acts as a molecular switch, cycling between on and off states by binding either guanosine triphosphate (GTP) or guanosine diphosphate (GDP). When bound to GTP, it undergoes conformational changes in its Switch I and Switch II regions to assume an active conformation whereby it can interact with various cellular proteins known as RAS effectors (2). The nucleotide-bound state and thus the activation state of RAS is regulated by guanine nucleotide exchange factors (GEFs) and GTPase activating proteins (GAPs) (3). GEFs activate RAS by promoting the exchange of GDP for GTP. Binding of GEFs weakens the GTPase's affinity for GDP. Since the cellular concentration of GTP is ten times that of GDP, increased GDP release promoted by GEFs will result in more GTP-bound RAS molecules (4). RAS has very slow intrinsic GTP hydrolysis activity (5). GAPs negatively regulate RAS by accelerating the rate of hydrolysis, thus promoting the inactive GDP-bound state (2). They do so by interacting with a glutamine residue (Q61; HRAS numbering) in the Switch II region of the GTPase, which is crucial to the hydrolysis reaction (6).

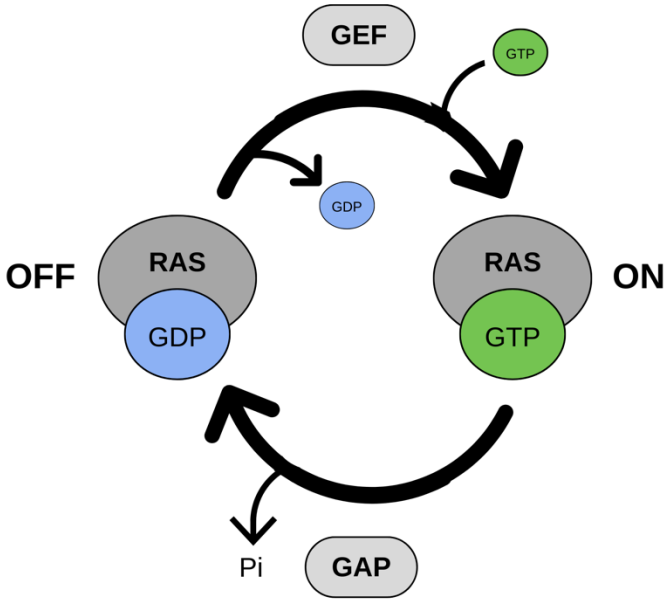

Figure 1. The GTPase cycle

RAS GTPases cycle between GTP-bound (active) and GDP-bound (inactive) states. GDP to GTP exchange is facilitated by GEFs, whereas GAPs promote the GDP-bound state by accelerating GTP hydrolysis.

There are more than 160 small GTPases of the RAS superfamily with conserved homologues in lower-level organisms and which control a very wide range of cellular processes (7). The RAS superfamily is divided into five subfamilies based on sequence homology and functional similarity: RAS, RHO, ARF, RAB, and RAN (8). RAS-subfamily proteins are thought to regulate cell proliferation, some functioning as oncogenes and others as tumor suppressors (9). RHO GTPases regulate cytoskeleton remodeling (10), ARF and RAB GTPases control trafficking (11,12) and a single RAN protein regulates nuclear import and export (13). The RAS-subfamily is composed of 35 proteins which share a high degree of homology, but which have very diverse roles in signal transduction.

The human genes *HRAS*, *NRAS*, and *KRAS* encode four protein isoforms: HRAS, NRAS, and the alternative splice variants KRAS4A and KRAS4B (2). All four isoforms have identical effector binding regions but differ in the 20 C-terminal residues termed hypervariable region (HVR) (14). The HVR is subject to lipid modifications, which are important for the plasma membrane (PM) localization of the protein. Evidence suggests that the isoforms are differentially located in specific membrane microenvironments. For example, HRAS and KRAS are found in cholesterol-rich lipid rafts (15,16). K/H/NRAS along with many other RAS GTPases possess a

CaaX motif at their C-terminus (where C is a cysteine, a is an aliphatic amino acid, and X is any amino acid). The CaaX motif is subject to prenylation at the cysteine by farnesyltransferases or geranylgeranyltransferases, and this prenylation is required for PM localization (17,18).

KRAS, HRAS, and NRAS have been intensely studied since their discovery more than five decades ago due to their prominent role in cancer (19,20). In fact, *K/H/NRAS* are the most mutationally activated oncogenes in human cancer, with a quarter of all cancer patients harboring activating mutations in one of these three genes (21). Activating mutations in K/H/NRAS-driven cancers typically occur at the glycine 12, glycine 13, or glutamine 61 residues, which trap the GTPase in the GTP-bound active conformation. Mutation of Q61 impairs both intrinsic and GAP-mediated hydrolysis, whereas mutation of G12 or G13 impairs GAP-mediated hydrolysis by preventing GAPs from accessing the site of GTPase activity (2). Mutations at G13 also result in increased GDP to GTP intrinsic exchange (21). Constitutively active K/H/NRAS mutants lead to cancer development and progression by signaling to pathways that promote growth and proliferation such as the mitogen-activated protein kinase (MAPK) pathway and the phosphatidylinositol 4,5-bisphosphate 3-kinase (PI3K) pathway (2).

RAS Effector Pathways

Signaling to K/H/NRAS is activated by binding of extracellular signaling molecules to receptor tyrosine kinases (RTKs). For example, binding of epidermal growth factor (EGF) activates the EGF receptor, leading to its phosphorylation at tyrosine residues. Upon receptor activation, the GEF SOS1 is recruited to the PM *via* the adaptor protein GRB2 where it will activate RAS by promoting the GTP-bound state (22). RAS will in turn engage its various downstream effectors, thus transducing the external stimulus to an intracellular functional response.

RAS interacts with effectors possessing RAS binding domains (RBDs) or RAS association (RA) domains. While RBD and RA domains possess low primary sequence similarity, they share a very similar ubiquitin-like tertiary structure, and their mode of interaction with RAS involving intermolecular interactions between anti-parallel β-sheets is the same for all effectors (23). There are more than 50 predicted RBD and RA domains in the human proteome (24).

The serine/threonine kinase RAF is the first RAS effector to be discovered and has been extensively investigated (25–27). RAF links RAS to the MAPK pathway, which drives gene expression and cell proliferation. The MAPK pathway consists of a cascade involving three

kinases: RAF, MEK, and ERK. Upon binding and PM-recruitment by RAS, RAF dimerizes and becomes active, subsequently phosphorylating MEK1/2, which in turn phosphorylate the MAPKs ERK1/2 (28). Phosphorylated ERK1/2 translocate to the nucleus where they phosphorylate and activates various proteins including transcription factors thus driving gene expression (29). There are three human isoforms of RAF: ARAF, BRAF, and CRAF (RAF1), which can bind K/H/NRAS with relatively high affinity. Activating *BRAF* mutations are observed in cancer, namely at the V600 residue (21). Activation of the RAF/MAPK pathway is critical in RAS-driven transformation (30), however, in most contexts, RAS requires activation of additional effector pathways to drive oncogenesis (31–33).

RAS can activate the PI3K pathway by binding to the catalytic p110α subunit of PI3 kinase, thus activating its kinase activity (34,35). Active PI3K leads to the accumulation of the PIP3 phospholipid at the PM, which recruits and activates the kinase AKT. AKT regulates several downstream pathways that promote cell growth and survival, cell cycle entry, metabolism, and inhibit apoptosis (36). The gene encoding PI3K p110α subunit (*PIK3CA*) is mutated in human cancer, and PI3K activation is necessary for RAS-driven transformation (33).

Another important family of RAS effectors are the RALGEFs (consisting of RALGDS and RGL1/2/3) that activate the RAS-family GTPases RALA and RALB (37). RALA/B can signal to several effectors, regulating functions such as trafficking, actin cytoskeleton organization and gene expression (38). As with RAF and PI3K, RAS signaling through RALGEFs is important for oncogenesis (39).

The effector Afadin (AFDN) links RAS to the maintenance of cell-cell contacts and cell polarity by interacting with the polarity protein Scribble (SCRIB) (40), whereas the tumor suppressor RASSF5 links RAS to the Hippo pathway (discussed below). Other RAS effectors include PLCε, and RIN1 (41,42). K/H/NRAS share their effectors with other RAS-family and RAS-superfamily GTPases, highlighting the plasticity of the GTPase/effector interaction (7).

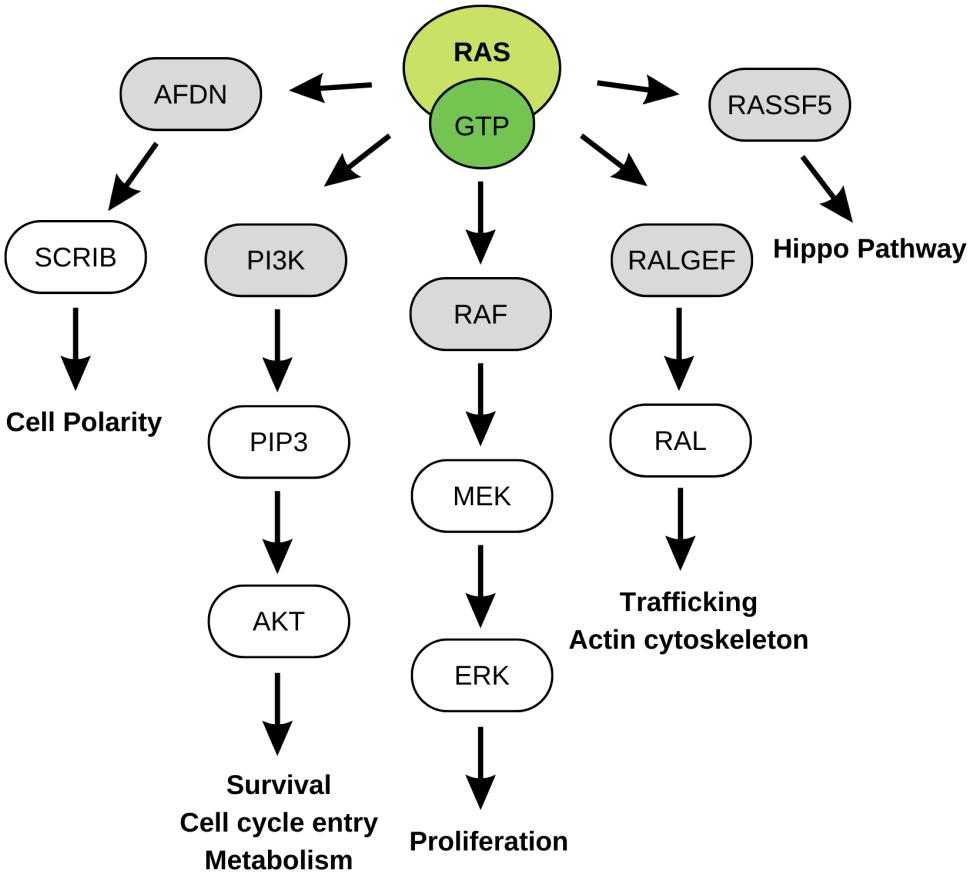

Figure 2. RAS effector pathways

When bound to GTP, RAS can interact with several effector proteins, thus activating various downstream signaling pathways. RAS engages RAF to activate the MAPK pathway, which promotes cell proliferation, whereas RAS activation of the PI3K pathway promotes cell growth and survival. Other RAS effectors include RALGEFs, AFDN, and RASSF5.

The role of RAS in Cancer

KRAS, *HRAS*, and *NRAS* are very frequently mutated in human cancers, particularly in colorectal (42% of cases), lung (20%), and pancreatic cancers (71%), which are among the most lethal and difficult to treat cancers (21,43).

The frequency of mutation of the isoform and the mutation itself vary depending on the cancer type. Among the three isoforms, most RAS mutations occur in KRAS. Furthermore, G12 is the residue most frequently mutated in KRAS-driven cancers. Specifically, 86% of pancreatic ductal adenocarcinomas (PDAC), 32% of lung adenocarcinomas (LUAD), and 41% of colorectal

cancers (CRC) harbor KRAS G12 mutations (most frequently G12D, G12V, or G12C) (21). NRAS is highly mutated at the Q61 residue in melanoma (29%). HRAS is less frequently mutated than the other two isoforms, but HRAS mutations at G12 and Q61 have been observed in head and neck squamous cell carcinomas and in bladder cancers (21).

Notably, many cancers that don't harbor RAS mutations, nonetheless have increased RAS signaling due to dysregulation of regulators such as upregulation of RTK expression/activation, gain-of-function of GEFs, or loss-of-function of GAPs (44,45). For example, the tumor suppressor NF1, which functions as a RASGAP, is very frequently inactivated in human cancer (2).

Oncogenic RAS signaling can drive cancer development and progression through different mechanisms. Namely, oncogenic RAS drives growth factor-independent cell proliferation by activating expression of genes that promote cell cycle progression *via* the MAPK, PI3K and RALGEF pathways, as well as suppresses apoptosis *via* the MAPK and PI3K pathways (46). Furthermore, oncogenic RAS can promote increased metabolism of tumors, immune evasion, and remodelling of the tumor microenvironment through processes such as increased angiogenesis. Additionally, RAS can promote metastasis by facilitating cell migration through various mechanisms, namely by disrupting cell-cell contacts, dysregulating the actin and tubulin cytoskeletons, and destabilizing the extracellular matrix (46).

Dysregulation of RAS signaling is also responsible for development of genetic disorders called RASopathies caused by germline mutations in the *RAS* genes as well as in genes encoding RAS regulators and effectors (45).

Development of targeted therapies to treat RAS mutant cancers has been ongoing for the last thirty years, with only mild success. Recently, sotorasib, a drug that directly targets $KRAS^{G12C}$ was approved for treatment of patients with non-small-cell lung cancer (NSCLC) (47). Sotorasib covalently binds GDP-bound $KRAS^{G12C}$ and prevents GDP to GTP exchange, thus preventing activation by SOS1 and association with RAF (48). This KRAS inhibitor is currently in numerous clinical trials for treatment of other $KRAS^{G12C}$-mutant cancers and for use in combination with other therapies (21). However, this inhibitor does not work on other KRAS mutations, including G12D or G12V, which are more common. In addition to development of drugs that directly target RAS, much research has focussed on developing inhibitors for RAS regulators such as SOS1, as well as inhibitors of RAS effectors such as RAF and PI3K. Several RAF and MEK inhibitors are currently approved for treatment of cancers driven by *BRAF* mutations, however, most of these

drugs are ineffective in treating RAS-driven cancers. Similarly, several PI3K inhibitors have been developed, however none are approved for use for RAS mutant cancers (21). While several promising therapies are currently in development (21), there remains a need for novel treatments and for the discovery of novel targets in RAS-driven cancers.

The Hippo pathway

Discovery of the Hippo pathway in *Drosophila*

Organ and tissue development is a tightly regulated process where cells must be capable of sensing the limits of the organ and changes in cell density. Thus, organ size control requires a careful balance between cell growth, cell-cycle progression, and apoptosis (49). A major pathway implicated in organ size control is the Hippo pathway.

The Hippo pathway was first discovered in *Drosophila* two decades ago. Mutational screens to identify genes whose loss-of-function leads to an overgrowth phenotype in flies identified the genes *Hippo* (*Hpo*), *Salvador* (*Sav*), and *Lats* (49,50). Inactivation of either of these three genes resulted in similar *Drosophila* phenotypes with overgrown organs exhibiting increased proliferation and decreased apoptosis (49–51). Further characterization revealed that Hpo, Sav, and Lats function as part of the same growth suppressive pathway whereby Hpo can bind and phosphorylate Sav, and that this Hpo/Sav interaction facilitates the phosphorylation of Lats (49,51).

The Hippo pathway genes are well conserved in mammals. Expression of the human homologue of Hippo in *Drosophila* can rescue the overgrowth phenotype caused by loss of Hpo (49). The organ size control function of this pathway is also conserved in mammals as dysregulating the Hippo pathway results in increased organ size in mice (52).

The Hippo pathway in mammals

The Hippo pathway in mammals is governed by a kinase cascade consisting of mammalian Ste20-like kinases (MST1) and MST2 orthologs of the *Drosophila* kinase Hippo, and of large tumor suppressor 1 (LATS1) and LATS2, mammalian orthologs of Lats. MST1/2 phosphorylate LATS1/2 which in turn phosphorylate Yes-associated protein (YAP) and transcriptional co-activator with PDZ-binding motif (TAZ) (53). This phosphorylation of YAP/TAZ at specific

serine residues (S127 and S89 respectively) creates binding sites for 14-3-3 proteins leading to their cytoplasmic sequestration (52,54,55). Additional phosphorylation sites on YAP/TAZ promote their ubiquitin-mediated degradation (56). The proteins SAV1 (mammalian homologue of Sav) and MOB1A/B function as adaptor proteins in this kinase cascade. Both SAV1 and MOB1 can be phosphorylated by MST1/2 and facilitate the MST/LATS interaction (50,57,58). When the Hippo pathway is inactive, YAP/TAZ are localized in the nucleus where they bind to transcription factors of the TEA domain (TEAD) family and activate expression of genes that promote growth and proliferation (52,56). Thus, the Hippo pathway negatively regulates growth and proliferation by regulating the nuclear localization and expression of YAP/TAZ.

Notably, the Hippo pathway is dysregulated in cancer as seen by an increase in YAP activity (53,59–62). Furthermore, multiple studies using mouse models show that dysregulation of Hippo pathway genes leads to tumorigenesis (53). NF2, a well characterized tumor suppressor, is a positive upstream regulator of the Hippo pathway (53). Furthermore, it was recently reported that loss of MST1/2 in KRAS-driven lung cancer drives tumor formation (63). Taken together, this evidence, along with evidence regarding the oncogenic function of YAP/TAZ (discussed below) highlights the importance of the Hippo pathway in cancer.

The MST1/2 kinases

The MST1 and MST2 kinases are at the core of the Hippo pathway. They are composed of an N-terminal kinase domain and of C-terminal coiled-coil motif termed Salvador-RASSF-Hippo (SARAH) domain. The SARAH domain mediates the dimerization of MST1/2, as the two coiled coils will bind in an antiparallel manner. Upon dimerization, which is further stabilized by SAV1 binding, the kinase will trans-autophosphorylate at a threonine residue in its activation loop (T183 for MST1 and T180 for MST2) and become active (50,64–67). MST1/2 are cytoplasmic, although they cycle through the nucleus. MST1/2 have been shown to be subject of cleavage by caspases in certain cell types (50).

The transcriptional co-activators YAP/TAZ

YAP and TAZ are two homologous transcriptional co-activators. They can bind to all four TEAD-family proteins, activating their transcription factor activity (56). YAP/TAZ have been

shown to promote expression of genes involved in cell proliferation including *MKI67*, *MYC*, and *SOX4*, and antiapoptotic genes such as *IAP* family and *BCL2* family genes, among others (52). YAP and TAZ are *bona fide* oncogenes. Amplification of the chromosomal region that contains the *YAP* gene is observed in various human cancers (60), and the *TAZ* encoding locus is amplified in a subset of breast cancers (68). YAP overexpression in various cell types can overcome contact inhibition (54), activate proliferation, inhibit apoptosis (52,69), and promote tumor formation (60,61). Both YAP and TAZ have been shown to activate epithelial-to-mesenchymal transition (EMT). Epithelial cells overexpressing YAP or TAZ display hallmarks of EMT such as having an invasive phenotype, upregulated mesenchymal markers, and disorganized adherens junctions (55,69). Furthermore, YAP can bind and activate the EMT-driving transcription factor FOS (62). EMT is an important process for cancer progression as it confers cancer cells of epithelial origin traits necessary for invasion and metastasis such as disruption of cell junctions and loss of cell polarity (70). Cell stemness is also a hallmark of cancer. In addition to activating EMT, TAZ can promote cancer stem cell-like properties in breast cancer such as self-renewal and tumorigenic potential (68).

The YAP oncogene seems to be very important in some KRAS-driven cancers. In mouse models of KRAS-driven pancreatic and lung cancers, tumors that have relapsed following KRAS inhibition show increased YAP activation (61,62). In KRAS-driven colorectal cancer cells, YAP expression can rescue proliferation following knock down of KRAS (62). Overexpression of YAP in a KRAS-driven breast cancer line promotes metastasis (71), and YAP and RAS cooperate to initiate tumorigenesis in rhabdomyosarcoma (72). Finally, YAP has increased activation in RAS-driven neuroblastoma following treatment with MEK inhibitors (73). Targeting YAP in RAS-driven cancers poses a very appealing therapeutic strategy to be pursued.

Upstream regulators of the Hippo pathway

The Hippo pathway is regulated by mechanical cues such as stretch and compression and by disruption of the actin cytoskeleton (74–77). Cell-cell adhesion regulates the Hippo pathway (78,79), and proteins at cell-cell contacts can sense mechanical cues and can transmit those signals to the Hippo pathway (80). Namely, disrupting α-catenin or E-cadherin, components of adherens junctions, activates YAP (81). Furthermore, cell polarity proteins can regulate the Hippo pathway. SCRIB positively regulates the Hippo pathway in epithelial cells by promoting assembly of the

MST/LATS/TAZ complex (68). Conversely, Discs large homolog 5 (DLG5), which is involved in maintenance of apicobasal cell polarity, negatively regulates the Hippo pathway by directly binding MST1/2 and preventing its interaction with LATS1/2 (82). Another Hippo pathway regulator is the tumor suppressor NF2. NF2 is localized at the plasma membrane and positively regulates the Hippo pathway by binding and activating LATS1/2 (53,83–85). Additionally, G-protein coupled receptors (GPCRs) can either activate or inhibit the Hippo pathway depending on the type of receptor. GPCRs with a Gα subunit of type G11, G12, G13, or Gq activate YAP by inhibiting LATS1/2 activity, whereas Gs-coupled receptors inhibit YAP by activating LATS1/2. The latter case likely involves RHO GTPases and actin cytoskeleton reorganization (86).The upstream regulation of the Hippo pathway is not as well characterized as the core kinase cascade, and the precise mechanisms regulating the Hippo pathway are likely context dependent.

Hippo pathway activation at the plasma membrane

There is convincing evidence that Hippo pathway signaling occurs at the plasma membrane. Yin *et al* have shown that both in *Drosophila* and in human cells, NF2 recruits LATS1/2 the plasma membrane and that this recruitment is important for activation of LATS1/2 (84). Similarly, membrane-targeted expression of MOB1A/B activates LATS1/2 (57). SAV1 is primarily membrane localized. Co-expression of SAV1 and MST1 promotes membrane-translocation of MST1 (84). *In vitro* simulation of membrane recruitment of MST1/2 increases their kinase activity by promoting their dimerization and autophosphorylation (66).

The RASSF family of RAS Effectors

RASSF proteins are effectors of RAS GTPases

The RAS association domain family (RASSF) consists of 10 scaffold proteins which play roles in inhibiting cell growth and survival and in promoting apoptosis. Like their name suggests, all ten family members contain an RA domain. The RA domain of RASSF1-6 (C-RASSFs) is located near the C-terminus, whereas that of RASSF7-10 (N-RASSFs) is at the N-terminus. Interestingly, only RASSF5 is a *bona fide* effector of H/N/KRAS, binding to the GTPase *via* its RA domain. A crystal structure of the RA domain of RASSF5 bound to HRAS has been solved, and the interaction has a dissociation constant of 80 nM (87). While some groups have reported

binding between KRAS and RASSF1 *in vitro*, the affinity of the interaction is extremely weak, and we and others have provided ample evidence demonstrating that RASSF1 is not an effector of KRAS in cells. When co-expressed, constitutively active KRAS and RASSF1 do not share the same cellular localization; RASSF1 is localized at microtubules whereas KRAS is present at the plasma membrane (**Fig 4**). In fact, RASSF1 seems to be an effector of other RAS-subfamily GTPases such as REM1/2, GEM, and RASL12 (88).

RASSF1 and RASSF5 are most closely homologous to each other among the ten RASSF proteins, with 66% sequence similarity, and are the best studied in this effector family.

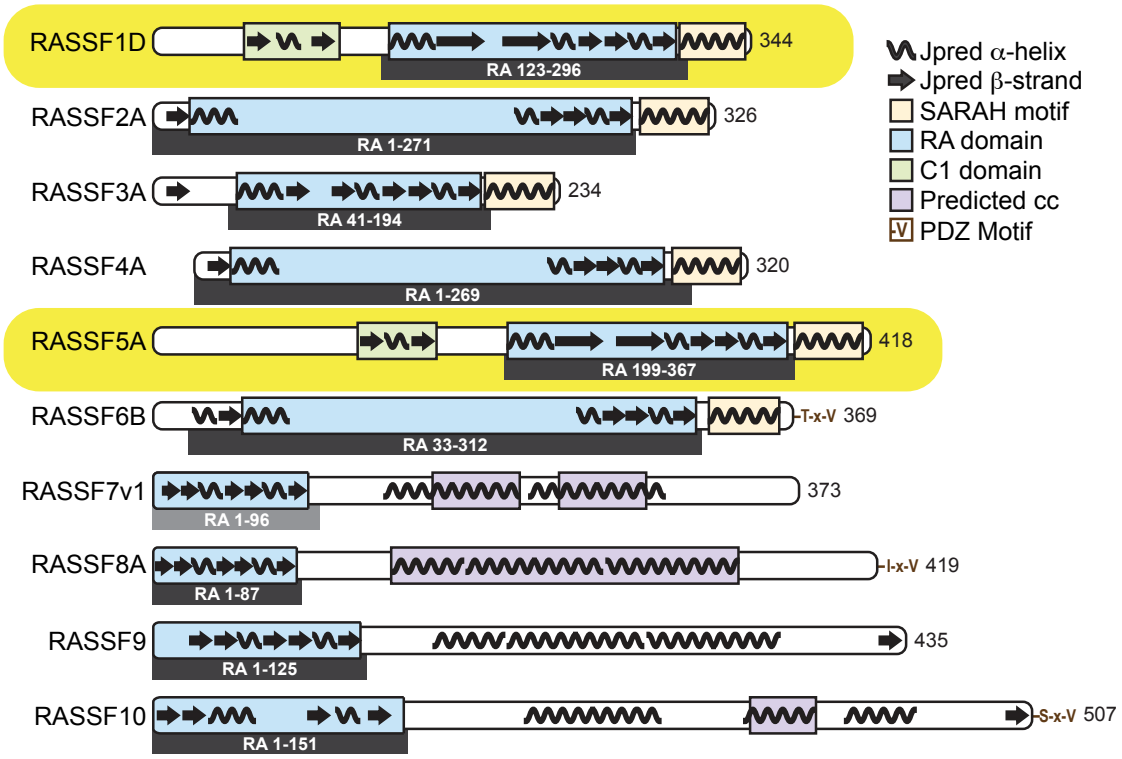

Figure 3. Schematic representation of the domain architecture RASSF family proteins

The RASSF family is composed of 10 proteins, all of which contain a RAS association (RA) domain, shown in blue. Jpred secondary structure predictions are shown. RASSF1-6 possess a C-terminal coiled-coil SARAH motif. SMART (Simple Modular Architecture Research Tool)–predicted coiled-coil (cc) domains of RASSF7-10 are in purple. This figure is adapted from (88).

The tumor suppressor role of the RASSF1 and RASSF5

The *RASSF* genes are epigenetically silenced in human cancer by promoter hypermethylation at GpG islands, most notably *RASSF1* which is the most frequently methylated

human gene (89–93). Notably, *RASSF1* is methylated in 90% of hepatocellular carcinomas, in 80% of small cell lung cancers, in 70% of prostate cancers, and in 60% of breast cancers (93). *RASSF1* is also downregulated in cancer *via* deletion of the chromosomal region where the gene is located, and is also occasionally mutated *via* point mutations (93). *RASSF5* is also frequently subject to promoter methylation (94,95).

The tumor suppressive role of RASSF1 and RASSF5 is well established. Overexpression of RASSF1 or RASSF5 in cancer cells has been shown to reduce growth and tumorigenicity in nude mice (89,90,96,97), and mice lacking *Rassf1* are more susceptible to developing tumors (93). Furthermore, RASSF1 and RASSF5 can promote death receptor ligand-induced apoptosis (97–102). Activation of apoptosis likely involves RASSF1 binding to the BAX-interacting protein MOAP1 (99). Additionally, RASSF1 can activate apoptosis downstream of MST1/2 (102,103), likely by phosphorylation and activation of the NDR1/2 kinases, which are of the same family as LATS1/2 (101).

Unlike RASSF5 which displays nuclear and cytoplasmic localization, RASSF1 can associate with and stabilize microtubules, including at the mitotic spindle. Due to its stabilizing function on microtubules, overexpression of RASSF1 leads to mitotic arrest in anaphase, by leading to loss of microtubule dynamics and improper mitotic spindle formation (104).

Binding between RASSF proteins and MST1/2

Like MST1/2, the C-RASSFs possess a C-terminal SARAH domain. Using this SARAH domain, all six C-RASSFs are capable of associating with MST1/2 (64,88,102,103). Furthermore, the RASSF SARAH domain can be used for homodimerization, or for heterodimerization between RASSF1 and RASSF5 (105). The only proteins that possess this well-conserved SARAH domain are the C-RASSFs, MST1/2, and SAV1. SAV1 associates with MST1/2 through its SARAH domain. NMR binding studies show that MST binding to SAV1 or RASSF5 is mutually exclusive and affinity of RASSF5 for MST1 is higher than that of SAV1 (106).

RASSF binding to MST1/2 inhibits their kinase activity by preventing their homodimerization and autophosphorylation *in vitro* (64,107). The main determinant of the kinase activity of MST1/2 is their phosphorylation state, and association with RASSF or SAV1 once they are already phosphorylated does not further modulate their activity (65,67). While RASSF1 and RASSF5 are well established to have an inhibitory effect on MST1/2 *in vitro*, their regulation of

the kinases and of the Hippo pathway *in vivo* is less clear. In fact, RASSF1 and RASSF5 are generally considered positive regulators of Hippo. We have shown that when constitutively active $KRAS^{G12V}$ is co-expressed with either RASSF1 or RASSF5, YAP becomes localized to the cytoplasm, indicating that the Hippo pathway is active (**Fig 4**) (88).

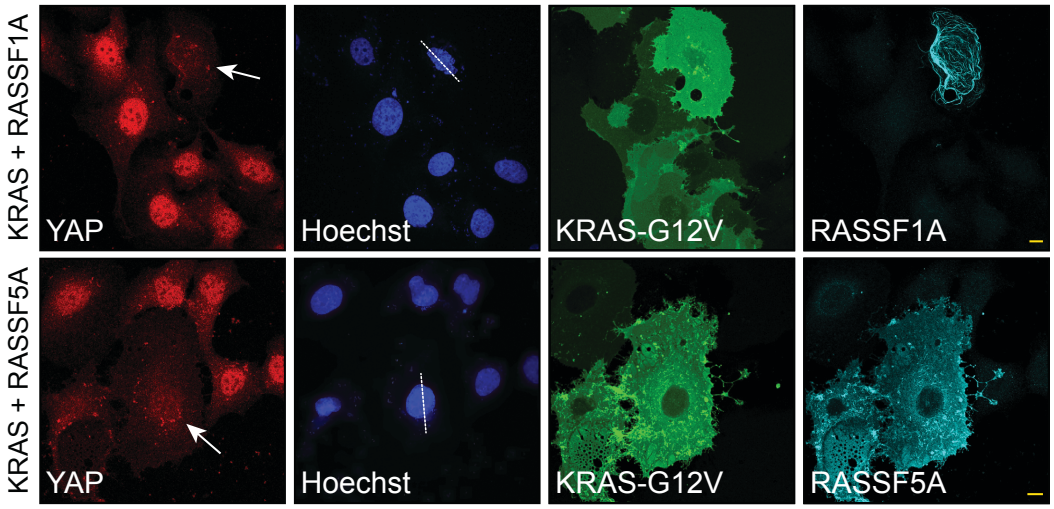

Figure 4. Co-expression of $KRAS^{G12V}$ with either RASSF1 or RASSF5 leads to Hippo pathway activation.

Immunofluorescence images of U2OS cells expressing Venus-$KRAS^{G12V}$ (green) and FLAG-RASSF1 or FLAG-RASSF5 (cyan). The activation state of the Hippo pathway is assessed by the subcellular localization of endogenous YAP (red). Scale bars are 10 μm. This figure is adapted from (88).

Hippo pathway regulation by the RASSFs

How can the inhibitory role of RASSF1/5 on MST activity *in vitro* be reconciled with their activating role on Hippo signaling? A hypothesis proposed by Praskova *et al* - the *reservoir model* - addresses this paradox. This model suggests that RASSF binding to MST stabilizes the kinase and creates reservoirs of inactive MST primed for activation once released by RASSF as a result of upstream signals (64). In line with this model, active KRAS would recruit RASSF5 to the plasma membrane, thus releasing MST and activating the Hippo pathway (**Fig 5**).

A second model - the *membrane complex model* - ignores the *in vitro* evidence regarding the inhibitory role of RASSF1/5 binding to MST. It proposes that when the Hippo pathway is active, KRAS, RASSF5, and MST1/2 form a complex at the plasma membrane. MST1/2

recruitment to the membrane activates the kinases by bringing them in close proximity to their substrates. This is in line with evidence suggesting that the Hippo kinase cascade occurs at the plasma membrane. Furthermore, Khokhlatchev *et al* have shown that when exogenously expressed in cells, $KRAS^{G12V}$ is able to co-precipitates both RASSF5 and MST1 (103).

A problem with both models is they assume KRAS binding and membrane-recruitment of RASSF, which is likely true for RASSF5, but fails to explain how RASSF1, which does not bind nor co-localize with KRAS, can activate the Hippo pathway upon co-expression with KRAS.

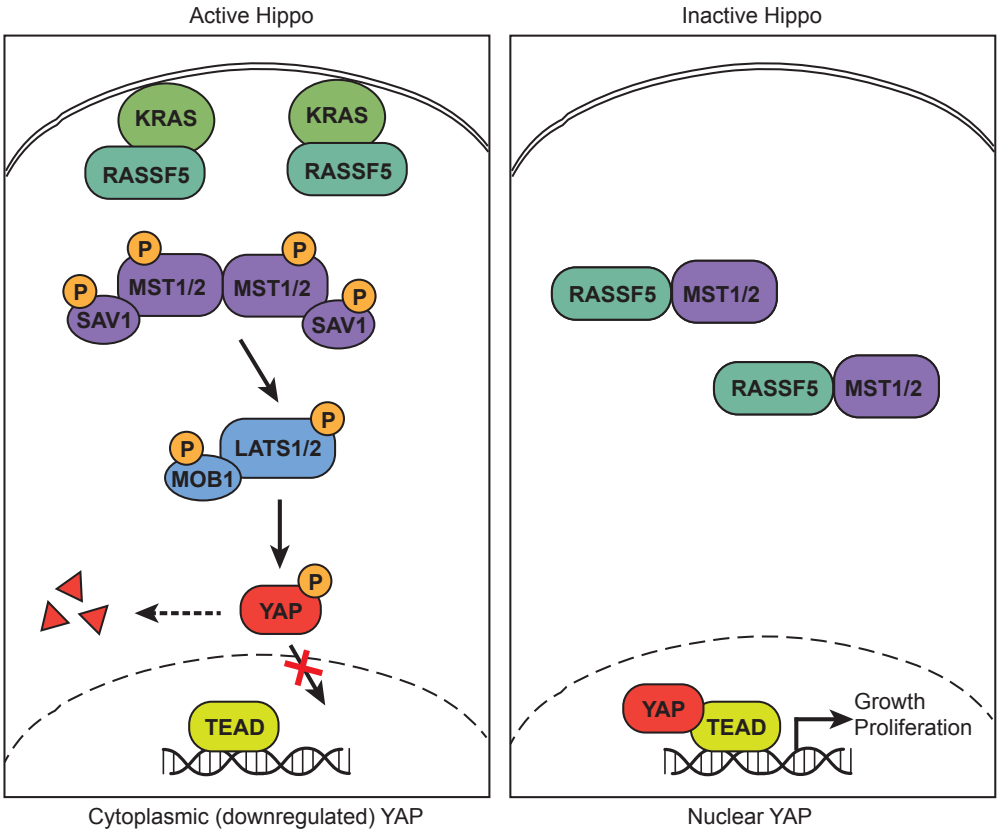

Figure 5. Schematic Representation of the Hippo Pathway in Mammals

When the Hippo pathway is active (left panel), the kinases MST1/2 phosphorylate LATS1/2, which in turn phosphorylate the transcriptional co-activator YAP. Phosphorylated YAP is sequestered to the cytoplasm and targeted for degradation. When the Hippo pathway is inactive (right panel), YAP is in the nucleus where it binds to TEAD family transcription factors and promotes expression of genes involved in growth and proliferation. Binding of RASSF1/5 to MST1/2 inhibits their kinase activity. KRAS might function to activate the Hippo pathway by sequestering RASSF5 to the plasma membrane.

Using a Rewiring Approach to Study RAS Signaling

RAS signaling to its various effector pathways is in part regulated by RAS's binding affinity towards its effectors and on their local concentration. By modifying RAS's affinity towards specific effectors, it is possible to modulate its output to downstream pathways. In the late 1990s, several HRAS mutants were discovered that preferentially bind to some effectors and were used to study RAS signaling downstream of these effectors.

$HRAS^{T35S}$ specifically activates the RAF/MAPK pathway (31), $HRAS^{E37G}$ binds RALGDS but is unable to bind RAF or PI3K (108), and $HRAS^{Y40C}$ interacts specifically with PI3K (33). These HRAS mutants helped to establish that multiple RAS effector pathways are necessary for RAS-mediated transformation and have played an important role in elucidating specific functions of the RALGDS and PI3K effector pathways (32,108–111). Interestingly, the $HRAS^{G12V/E37G}$ mutant has also been reported to bind RASSF5 and is able to induce apoptosis *via* RASSF5 more efficiently than $KRAS^{G12V}$ (103).

The $KRAS^{I21F/H27R}$ mutant

KRAS binds to the effector BRAF with a 30-fold greater affinity than to RASSF5 (**Fig 6C**), making it difficult to study the effect of RAS signaling solely on the Hippo pathway. We sought to design a rewiring mutant of KRAS that would signal preferentially downstream of the effector RASSF5.

By comparing the crystal structures of HRAS bound to either BRAF or RASSF5, we identified mutations that abrogate the HRAS/BRAF interaction or enhance the HRAS/RASSF5 interaction. These mutations are grouped in two hotspots: A66D, E37D, M67W which are predicted to weaken the interaction with BRAF, and I21F, Q25Y, H27R which are predicted to increase the interaction with RASSF5 (**Fig 6B**).

Pulldown assays with GST-tagged KRAS mutants and purified RA domains of BRAF and RASSF5 show that $KRAS^{I21F}$ and $KRAS^{H27R}$ are successful in increasing binding with RASSF5. Isothermal titration calorimetry (ITC) experiments with a double mutant of KRAS possessing both mutations ($KRAS^{I21F/H27R}$) reveal that $KRAS^{I21F/H27R}$ has 4.5-fold reduced affinity for BRAF and 2-fold increased affinity for RASSF5, compared to $KRAS^{WT}$. Overall the difference in affinity between $KRAS^{I21F/H27R}$:BRAF (270 nM) and $KRAS^{I21F/H27R}$:RASSF5 (1000 nM) is only 3-fold, as

opposed to 30-fold for KRAS^{WT} (**Fig 6C**). We reasoned that this KRAS$^{I21F/H27R}$ rewiring mutant could be used to study the effect of KRAS signaling downstream of RASSF5 and to the Hippo pathway, with diminished activation of the MAPK pathway.

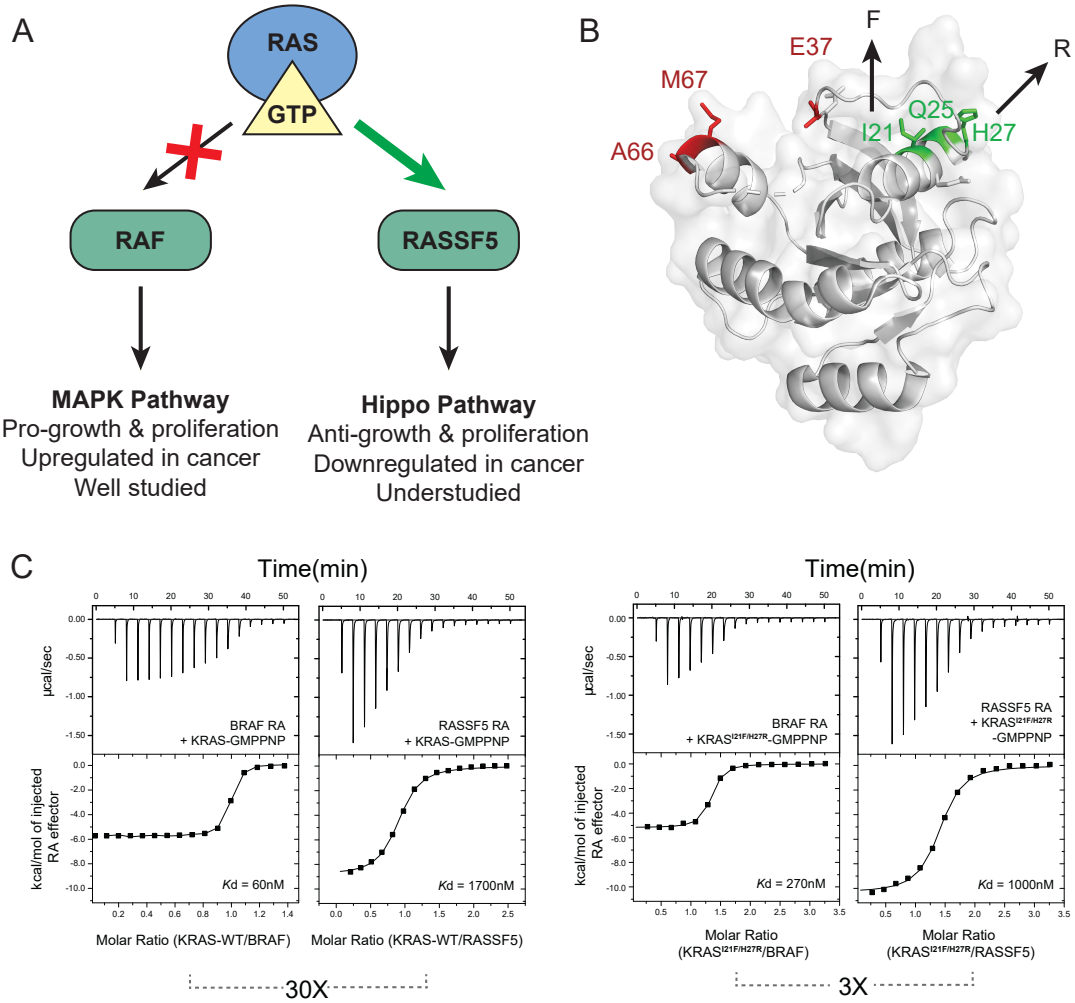

Figure 6. KRAS$^{I21F/H27R}$ is a rewiring mutant to RASSF5

(A) Schematic representation of rewiring of KRAS to RASSF5. A KRAS mutant with increased specificity for RASSF5 can be used to study KRAS signaling downstream of RASSF5 (e.g. to the Hippo pathway), in the context of decreased MAPK signaling. (B) Structure of HRAS showing amino acid residues computationally predicted to differentially impact KRAS interaction with BRAF and RASSF5. Mutating residues I21 and H27 has the greatest effect on RAS rewiring. (C) Isothermal titration calorimetry (ITC) data showing binding of either KRAS^{WT} or KRAS$^{I21F/H27R}$ to the BRAF or RASSF5 RA domains. The difference in binding affinity of KRAS$^{I21F/H27R}$ to BRAF versus RASSF5 is only 3-fold, as opposed to a 30-fold difference for KRAS^{WT}.

The RASSF1^{NCKL} mutant

Despite not binding KRAS directly, the RA domain of RASSF1 is highly similar to that of RASSF5; only a few residues at the RASSF5/RAS binding interface differ in RASSF1 (**Fig 7A**) (88). We compared the RASSF1 and RASSF5 RA domains to identify mutations in RASSF1 that increase its affinity for KRAS. A cysteine in the αN helix of the RA domain of RASSF5 creates an important hydrophobic interaction with a tyrosine in the switch II region of HRAS. We mutated the corresponding asparagine in RASSF1 to a cysteine (N149C). ITC experiments reveal that RASSF1^{N149C} has detectable binding with KRAS, with a dissociation constant of 9.4 μM (**Fig 7B**) (88).

Furthermore, a lysine (K208) in the β2-sheet of the RA domain of RASSF1 is predicted to cause steric hindrance with HRAS. A double mutant of RASSF1-RA containing both mutations predicted to increase affinity with KRAS (RASSF1$^{N149C/K208L}$, hereafter referred to as RASSF1^{NCKL}) is indeed capable of precipitating KRAS^{G12V} in GST-pulldown assays, and the RASSF1^{N149C} single mutant also shows binding to KRAS^{G12V}, to a lesser extent (**Fig 7C**). Microscopy images reveal that co-expression of RASSF1^{NCKL} with KRAS^{G12V} in U2OS cells can activate the Hippo pathway, as observed by staining for YAP (**Fig 7D**). Interestingly, whereas RASSF1 is localized at microtubules (**Fig 4**), RASSF1^{NCKL} has nuclear localization like RASSF5, and when co-expressed with KRAS^{G12V}, RASSF1^{NCKL} completely co-localizes with the GTPase. The rewired RASSF1^{NCKL} mutant likely conserves many of the cellular functions specific to the RASSF1 effector, while being able to associate to KRAS. Thus, we expect that RASSF1^{NCKL} can be used to study the role of RASSF binding to KRAS in activating the Hippo pathway.

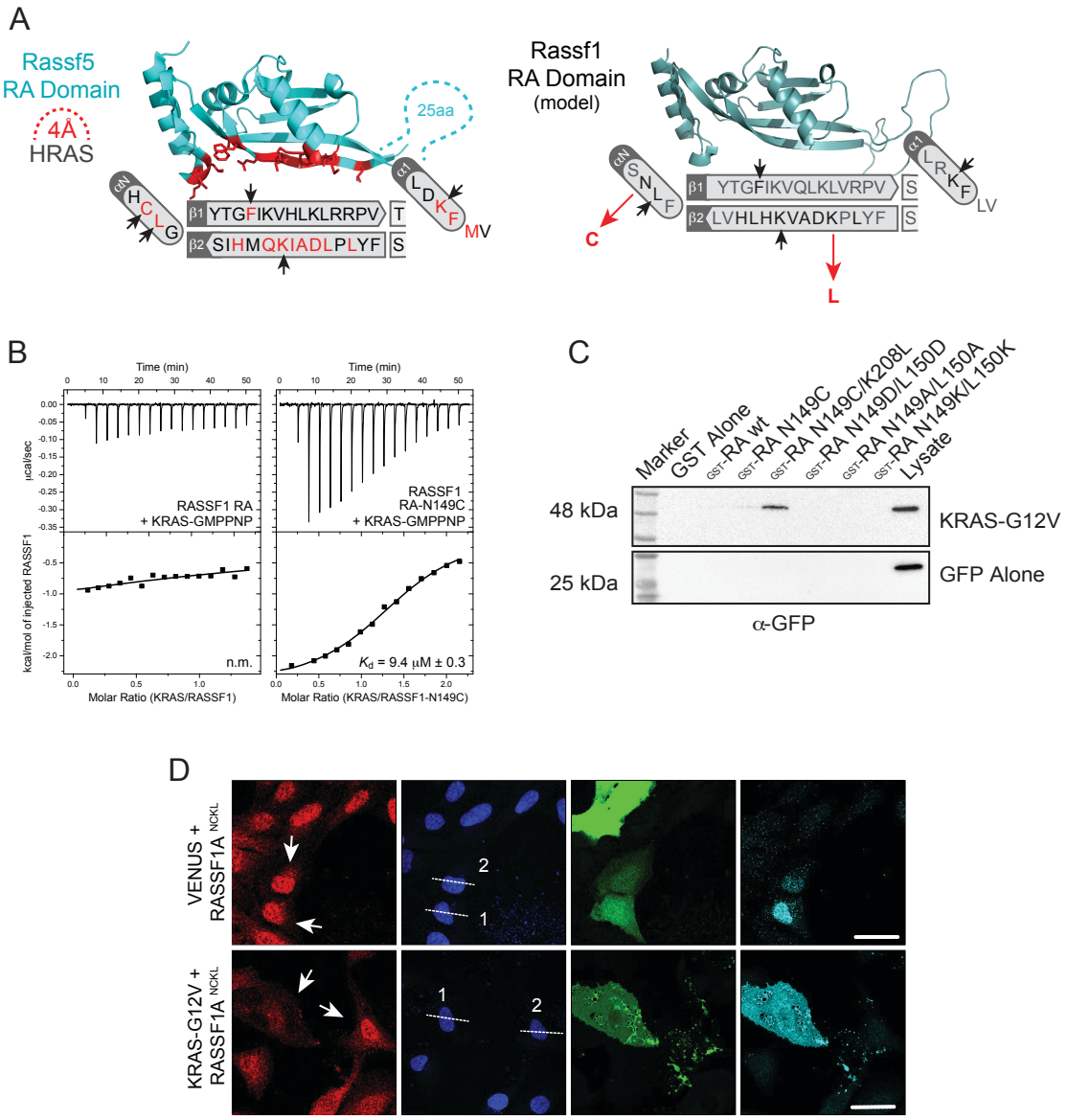

Figure 7. RASSF1^{NCKL} mutant is capable of binding KRAS

(A) Ribbons representations of the RA domain of RASSF5 (PDB 3DDC) and of a model of the RA domain of RASSF1. Residues found at the binding interface with HRAS are shown below the structures. Residues in red are those within 4 Å of HRAS. Residues indicated by black arrows are those predicted to make interactions with HRAS (88). (B) Isothermal titration calorimetry (ITC) data showing binding of KRAS with either RASSF1^{WT} or RASSF1^{N149C} RA domains. The RASSF1^{N149C} mutant binds KRAS with an affinity of 9.4 μM, whereas no binding is detected between wild-type RASSF1 and KRAS. (C) GST-tagged RASSF1 RA domain mutants were purified on glutathione beads and incubated with cell lysates expressing GFP-tagged KRAS^{G12V}. RASSF1$^{N149C/K208L}$ RA domain displays binding with KRAS^{G12V}, and the RASSF1^{N149C} RA domain also displays binding, although much weaker. (D) Immunofluorescence images of U2OS

cells showing co-localization of Venus-KRAS^{G12V} (green) and FLAG-RASSF1$^{N149C/K208L}$ (cyan). The activation state of the Hippo pathway is assessed by the subcellular localization of endogenous YAP (red). Scale bars are 35 μm. This figure is adapted from (88).

BioID proximity biotinylation

BioID is a proteomic technique used to identify proximal interactors of a protein of interest (bait). The bait is fused to a mutant *Escherichia coli* biotin protein ligase (BirA*) and the BirA*-bait recombinant protein is expressed in living cells (112). BirA* catalyzes a reaction with biotin generating a reactive biotinyl-AMP intermediate. Biotinyl-AMP reacts with epsilon amine groups of exposed lysine residues of proteins that come in an approximate 10 nm radius of the BirA*-bait (although this radius can vary depending on the cellular compartment), resulting in their biotinylation (113).

Biotinylated targets can be affinity purified using streptavidin beads, digested with trypsin, and identified by mass spectrometry, revealing the interaction network (interactome) of the bait (112) (**Fig 8A**). BioID has several advantages over other interactome-mapping techniques *e.g.,* affinity purification mass spectrometry (AP-MS), such as its ability to capture weak and transient interactions *in vivo*. Due to mixing of proteins from different cellular compartments during cell lysis, AP-MS might identify interactions that do not normally occur *in vivo*. Furthermore, since BioID relies on biotinylation, which is a covalent modification, more stringent lysis can be employed, thus allowing for identification of proteins found in poorly soluble cellular compartment, such as membranes, chromatin, the nuclear lamina, and the cytoskeleton (113).
Not only can the BioID technique be used to map the interactome of a single protein, but it can also be used to systematically map the composition and organization of entire cellular compartments, including membrane-less organelles that cannot be efficiently isolated by fractionation (114–116). Recently, Go *et al* have used BioID to map an extensive interactome of HEK 293 cells by using 234 baits localized in more than 30 cellular compartments (117).

BioID results in the identification of thousands of hits, most of which are not true proximity partners of the bait. For example, endogenously biotinylated proteins such as mitochondrial carboxylases, proteins that are non-specifically biotinylated by most baits, and proteins that bind non-specifically to Sepharose beads will be among the hits. It is therefore crucial to use appropriate controls (**Fig 8B**). Cells not expressing the BirA* enzyme can be used to control for endogenously

biotinylation, and the BirA* enzyme expressed alone or fused to a control such as green fluorescent protein (GFP) can be used to control for promiscuous biotinylation (113).

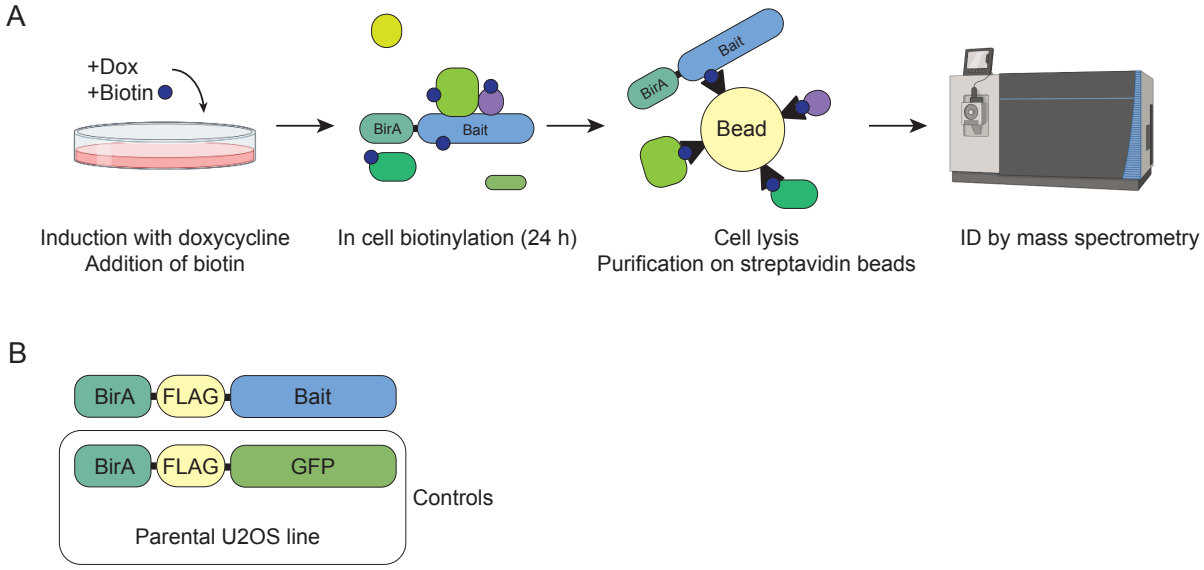

Figure 8. Schematic illustration of the BioID technique.

(A) BioID is a proteomic technique which allows identification of proximal interactors of a bait protein. The bait is fused to a mutant biotin ligase (BirA*) and expressed in cultured cells. Upon addition of biotin, proteins proximal to the bait become biotinylated, and can thus be purified on streptavidin beads and identified by mass spectrometry. (B) Two negative controls were used; the parental cell line to control for endogenous biotinylation, and BirA* coupled to GFP to control for non-specific biotinylation.

Rationale and Objectives

While the literature points to a clear link between KRAS, RASSF proteins, and the Hippo pathway, there are significant gaps in knowledge in explaining the precise mechanisms by which KRAS and RASSF1/5 activate Hippo signaling.

(a) KRAS signaling downstream of its effectors RAF and PI3K is very well elucidated. By contrast, the signaling which occurs downstream of KRAS engaging its effector RASSF5 is poorly understood. How KRAS/RASSF5 signaling activates apoptosis either *via* the Hippo pathway or *via* other pathways is unclear.

(b) While the core Hippo kinase cascade and its regulation of YAP/TAZ is well understood, the upstream regulation of this pathway is not as well characterized. Some mechanisms by which cellular cues such as cell-cell contact, polarity, and actin cytoskeleton dynamics regulate the Hippo pathway are gradually being elucidated. However, it is unknown how these Hippo regulators might couple to RAS signaling.

(c) It is still not entirely clear how the RASSF proteins themselves regulate the Hippo pathway *in vivo*. Their inhibitory function on MST1/2 kinases *in vitro* seemingly conflicts with their requirement for Hippo pathway activation.

(d) RASSF1 cooperates with KRAS to activate the Hippo pathway, despite not being a KRAS effector. This KRAS/RASSF1 cooperation is thus indirect and can only be explained by the involvement of other proteins.

The rationale behind this M.Sc. thesis is to address some of the knowledge gaps outlined in the above four points in hopes of defining the precise mechanism of KRAS activation of the Hippo pathway *via* the RASSFs. We hypothesized that other proteins involved in this mechanism can be uncovered by BioID. The first objective of this project is to map the interactome of KRAS, RASSF1, and RASSF5 either alone or when co-expressed using BioID. The second objective is to validate some of the identified partners as true interactors.

MATERIALS AND METHODS

DNA constructs

Table 1: Expression constructs used in this study

Construct	Backbone	Cloning
BirA*-FLAG-eGFP	N-pSTV6	Gateway
BirA*-FLAG-KRAS	N-pSTV6	Gateway
BirA*-FLAG-KRAS G12V	N-pSTV6	Gateway
BirA*-FLAG-KRAS G12V/I21F/H27R	N-pSTV6	Gateway
BirA*-FLAG-RASSF1A	N-pSTV6	Gateway
BirA*-FLAG-RASSF1A N149C/K208L	N-pSTV6	Gateway
BirA*-FLAG-RASSF5A	N-pSTV6	Gateway
FLAG-KRAS G12V	pDEST-pcDNA5-FLAG-5’	Gateway
FLAG-KRAS G12V/I21F/H27R	pDEST-pcDNA5-FLAG-5’	Gateway
FLAG-RASSF5A	pDEST-pcDNA5-FLAG-5’	Gateway
3xFLAG-RASSFA	pMSCV-3xFLAG	Restriction
3xFLAG-RASSF1A N149C/K208L	pMSCV-3xFLAG	Restriction
3xFLAG-RASSF5A	pMSCV-3xFLAG	Restriction
3xHA-KRAS	pDEST-pcDNA5-3xHA-5’	Gateway
3xHA-KRAS G12V	pDEST-pcDNA5-3xHA-5’	Gateway
3xHA-KRAS G12V/I21F/H27R	pDEST-pcDNA5-3xHA-5’	Gateway
3xHA-SNAP23	pDEST-pcDNA5-3xHA-5’	Gateway
3xHA-VAMP3	pDEST-pcDNA5-3xHA-5’	Gateway
GFP-RASSF5A	pDEST-pLenti-CMV-GFP-Neo	Gateway
Venus-RASSF5A	pDEST-pcDNA3-Venus-5'	Gateway

N-pSTV6, pDEST-pcDNA5-FLAG-5’, and pDEST-pcDNA5-3xHA-5’ backbone vectors were graciously provided by Dr. Anne-Claude Gingras (LTRI, Toronto).

Cloning of the constructs shaded in grey was performed by me using Gateway recombination (Invitrogen). PCR primers with Gateway recombination sites were designed to PCR amplify gene sequences.

Table 2: PCR primers used for Gateway recombination cloning

Gene	Gene ID	Residues	PCR primers
RASSF1A	11186	Full length	Forward: GGGGACAAGTTTGTACAAAAAAGCAGGCTCCATGTCG GGGGAGCCTGAGCTCATTGAG Reverse: GGGGACCACTTTGTACAAGAAAGCTGGGTCCCCAAGG GGGCAGGCGTGCAGGG
RASSF5A	83593	Full length	Forward: GGGGACAAGTTTGTACAAAAAAGCAGGCTCCATGGCC ATGGCGTCCCCGGCCATCGGG Reverse: GGGGACCACTTTGTACAAGAAAGCTGGGTCCCCAGGT TTGCCCTGGGATTCTC
KRAS (KRAS4B)	3845	Full length	Forward: GGGGACAAGTTTGTACAAAAAAGCAGGCTCCATGACT GAATATAAACTTGTGGTAGTT Reverse: GGGGACCACTTTGTACAAGAAAGCTGGGTCTTACATA ATTACACACTTTGTCTTTGAC
SNAP23	8773	Full length	Forward: GGGGACAAGTTTGTACAAAAAAGCAGGCTCCATGGAT AATCTGTCATCAG Reverse: GGGGACCACTTTGTACAAGAAAGCTGGGTCTTAGCTGT CAATGAGTTTCTTTG
VAMP3	9341	Full length	Forward: GGGGACAAGTTTGTACAAAAAAGCAGGCTCCATGTCT ACAGGTCCAACTGC Reverse: GGGGACCACTTTGTACAAGAAAGCTGGGTCTCATGAA GAGACAACCCACAC

Genes were first cloned into a pDONR221 entry vector, and subsequently recombined in the indicated destination vectors. Constructs were validated by Sanger sequencing and by digestion with restriction enzymes followed by separation on a 0.8% agarose gel.

Cell culture and transient transfection

HEK 293T cells (ATCC CRL-1573) were maintained in Dulbecco's Modified Eagle Medium (DMEM) supplemented with 8% Newborn Calf Serum (NCS) and 2% Fetal Bovine Serum (FBS). U2OS cells (ATCC HTB-96) were maintained in DMEM supplemented with 10% FBS. Cells were maintained at 37 °C and were passaged every 3-4 days to maintain a confluency of 30-95%. Transient transfection in HEK 293T cells was performed using Polyethyleneimine (PEI), whereas transient transfection in U2OS was performed using Lipofectamine (Thermo Fisher Scientific). Cells were seeded in either 6-well plates or 6 cm plates at approximated 0.5 million or 1 million cells per well and grown for 24 hours prior to transfection, and 2μg or 4μg of DNA was transfected.

Lentiviral infection

At 75% confluency, HEK 293T cells were transfected with second generation lentiviral packaging and envelope expression vectors (psPAX2 and pCMV-VSV-G) together with one of the N-pSTV6 BioID expression vectors. After 24 hours, media was replaced with media containing 5% FBS and 100 μg/mL penicillin/streptomycin. After a subsequent 24 hours, media containing the lentivirus was collected and filtered through a 0.45 μm filter. U2OS cells at 30% confluency in 10 cm plates were infected with lentivirus; 2.5 mL of virus-containing media was added per 10 cm plate. Polybrene at a final concentration of 8 μg/mL was also added to the media. After 24 hours, 2 μg/mL puromycin was added to the infected cells, to select for stably expressing clones. Antibiotic selection was maintained for 3-5 days, during which cells were scaled up to 15 cm plates. To determine the amount of lentivirus to be used for efficient infection, viral titering was performed. U2OS cells plated in a 6-well plate were infected with varying amounts of virus-containing media expressing the N-pSTV6-GFP vector, ranging from 125 μL to 500 μL per well. GFP fluorescence was assessed under the microscope to estimate the percentage of infected cells

48 hours following infection. The viral titre resulting in efficient infection (70%) was determined to be 500 µL per well (2.5 mL per 10 cm plate).

Generation of stable Flp-In T-REx cell lines

At 80% confluency, Flp-In T-REx (Invitrogen) U2OS cells (provided by Dr. Marc Therrien) in 6-well plates were transfected with Flp-Recombinase expression vector (pOG44), and with one of the pDEST-pcDNA5-FLAG-5'expression vectors. After 48 hours, 100 µg/mL hygromycin was added to the media to select for stably expressing clones. Antibiotic selection was maintained for 14 days, during which cells were scaled up to 15 cm plates.

Cell lysis

Prior to lysing, cells were washed twice with ice-cold Phosphate Buffered Saline (PBS), collected in PBS using a cell scraper, transferred to 1.5 mL Eppendorf tubes, and pelleted by centrifugation at 500 x g for 5 mins at 4 °C. For all experiments except BioID, cells were lysed in 200-300 µl of Lysis Buffer (20 mM Tris-HCl pH 7.4, 150 mM NaCl, 5 mM $MgCl_2$, 10% Glycerol, 1% TritonX-100, 2 mM DTT, Protease inhibitors (Sigma), 1 mM PMSF) for 10 mins at 4 °C. Lysates were clarified by centrifugation at 20,627 x g for 20 mins. The lysates were diluted in 6X SDS Sample Buffer (375 mM Tris-HCl pH 6.8, 60% Glycerol, 12% SDS, 0.6 M DTT) and then incubated at 95 °C for 5 mins.

SDS-PAGE and immunoblotting

Polyacrylamide gels (10%, 12% or 15%) were used for SDS-PAGE separation. Protein samples were electrophoresed at 180V for 1 hour in SDS running buffer (25 mM Tris base, 192 mM Glycine, 0.1% SDS). Subsequently, separated proteins were transferred to nitrocellulose membranes (Fisher Scientific) by wet transfer at 100V for 1 hour in Towbin buffer (25 mM Tris base, 192 mM Glycine, 20% methanol) at 4 °C. Membranes were blocked for 1 hour at RT with rocking in Tris-buffered saline Tween-20 (TBS-T) containing 5% skim milk. Membranes were incubated with primary antibody overnight at 4 °C with rocking, and then washed 3 times with TBS-T. HRP-conjugated secondary antibody was added for 1 hour at RT with rocking. Following

3 washes with TBS-T, ECL substrate (Bio-Rad) was added to the membranes, which were developed either on ChemiDoc imaging system (Bio-Rad) or on film.

Antibodies

All primary antibodies for immunoblotting were diluted in TBS-T containing 3% Bovine Serum Albumin (BSA) and 0.02% sodium azide. Primary antibody solutions were stored at 4 °C. All secondary antibodies were diluted in TBS-T alone.

Table 3: Antibodies used for immunoblotting and immunoprecipitation experiments

Antibody	Dilution	Source
anti-BRAF	1:500	Santa Cruz sc-5284
anti-FLAG	1:1000	Sigma F3165
anti-GAPDH	1:500	Sigma-Aldrich MAB374
anti-GFP	1:5000	Abcam ab290
anti-HA	1:1000	Santa Cruz sc-7392
anti-RAF1	1:2000	BD Biosciences 610152
anti-γTubulin	1:5000	Sigma T6557
Streptavidin-HRP conjugate	1:10000	GE Healthcare GERPN1231

Immunoprecipitation

For immunoprecipitation (IP), a 20 μL bed volume of Protein G Sepharose beads (Sigma-Aldrich) and 1-2.5 μg of antibody were used per sample. Sepharose beads were incubated with antibody for 1 hour at 4 °C with rotation. Subsequently, beads bound to antibody were washed 3 times with lysis buffer and cell lysates were incubated with the beads for 1-2 hours at 4 °C with rotation. The beads were pelleted (400 x g, 1 min), the supernatant removed, and beads were gently washed 3 times with lysis buffer. Following the last wash, 20 μL of 2X SDS Sample Buffer was added to the bead pellet, which was then incubated at 95 °C for 5 mins.

BioID and streptavidin purification

BioID was done using U2OS cells stably expressing BirA*-FLAG fusion proteins grown in 2 15 cm plates. At 75-80% confluency, cells were treated with 1 μg/mL doxycycline and 50 μM

biotin for 24 hours. Cells were lysed in Modified RIPA buffer (50 mM Tris-HCl pH 7.4, 150 mM NaCl, 1 mM $MgCl_2$, 1% NP-40, 0.5 mM EDTA, 1 mM EGTA, 0.4% SDS, protease inhibitors (Sigma), 1 mM PMSF, and 0.4% sodium deoxycholate) in a 4:1 volume:mass ratio. One µL of benzonase nuclease (250U; Sigma-Aldrich) was added to each sample and lysates were incubated for 30 mins at 4°C with rotation. Lysates were centrifuged for 20 min at 20,627 x g, and then incubated with 20 µL bed volume of streptavidin-sepharose beads (Sigma-Aldrich) pre-washed with Modified RIPA buffer. Affinity purification was performed overnight at 4°C with rotation. Beads were pelleted (400 x g, 1 min), the supernatant removed, and the beads were washed 1 time with 0.5 mL SDS-Wash buffer (25 mM TRIS-HCl pH 7.4, 2% SDS), 2 times with 0.5 mL RIPA-Wash buffer (50 mM Tris-HCl pH 7.4, 150 mM NaCl, 1% NP-40, 1 mM EDTA, 0.1% SDS, 0.4% sodium deoxycholate), 1 time with 0.5 ml TNNE-Wash buffer (25 mM TRIS pH 7.4, 150 mM NaCl, 0.1% NP-40, 1 mM EDTA), and 3 times in 0.5 mL 50 mM ammonium bicarbonate (ABC).

Trypsinization and analysis by mass spectrometry

Trypsinization and analysis by mass spectrometry was performed by the IRIC proteomics core facility. Samples were reconstituted in 50 mM ABC with 10 mM TCEP (Tris(2-carboxyethyl)phosphine hydrochloride; Thermo Fisher Scientific) and vortexed for 1 hour at 37°C. Chloroacetamide (Sigma-Aldrich) was added for alkylation to a final concentration of 55 mM. Samples were vortexed for another hour at 37°C. One microgram of trypsin was added, and digestion was performed for 8 h at 37°C. Samples were dried down and solubilized in 5% ACN-0.2% formic acid (FA). Peptides were loaded and separated on a home-made reversed-phase column (150-µm i.d. by 200 mm) with a 56-min gradient from 10 to 30% ACN-0.2% FA and a 600-nl/min flow rate on an Easy nLC-1000 connected to an Orbitrap Fusion (Thermo Fisher Scientific, San Jose, CA). Each full MS spectrum acquired at a resolution of 60,000 was followed by tandem-MS (MS-MS) spectra acquisition on the most abundant multiply charged precursor ions for a maximum of 3s. Tandem-MS experiments were performed using collision-induced dissociation (CID) at a collision energy of 30%.

BioID Data Analysis

The RAW data files generated by mass spectrometry were converted to an MGF format using RawConverter (118) and then searched using the search engine X!Tandem (119). Spectra

were searched against the human proteome from UniProt (https://www.uniprot.org/proteomes/UP000005640) and common contaminants from the Global Proteome Machine (GPM; http://www.thegpm.org/crap/index.html). The search results were uploaded to ProHits-Virtual Machine (120), for analysis. Four control runs were used for comparative purposes: 2 runs of a BioID analysis conducted on an unrelated bait protein (GFP) to control for non-specific biotinylation of intracellular proteins, and 2 runs from a BioID analysis conducted on wild-type U2OS cells to mimic the condition in which endogenous biotinylation (which primarily occurs on mitochondrial carboxylases) would be predominant. Each negative control was analyzed in biological replicates with 2 independent biological replicates per type of control. For visualization and comparison purposes, the spectral abundance of each hit was normalized. The normalization method used is described by Zybailov *et al* (121). For each hit in each BioID dataset, the number of identified spectra was divided by the protein length. This ratio was further divided by total number of spectra identified in the BioID, and then by the maximum value in the dataset.

Statistical Tests

The algorithm Significance Analysis of Interactome (SAINT), which computes which interactions can be deemed as statistically significant, was used to analyze the BioID datasets against the controls. SAINT assigns a confidence score to each identified interaction based on the spectral abundance of the prey in the control datasets, as well as in all datasets analyzed. Only hits that had more than one unique peptide identified and that had an X!Tandem value $\leq$-35 (corresponding to an FDR$\leq$0.01) were used for statistical analysis by SAINTexpress (version 3.6.1) (122). The more datasets are analyzed simultaneously by SAINT, the more stringent the SAINT score will be. A SAINT score of 0.9 corresponds to a FDR of 0.02 (122).

RESULTS

Validation of the rewiring mutants in cells

Having shown that the rewiring mutant of KRAS ($KRAS^{I21F/H27R}$) and that of RASSF1 ($RASSF1^{NCKL}$) work as designed *in vitro*, we sought to test their ability to interact with targets in cells. We transiently co-expressed HA-tagged $KRAS^{WT}$, $KRAS^{G12V}$, or $KRAS^{G12V/I21F/H27R}$ with FLAG-tagged RASSF5, $RASSF1^{WT}$, $RASSF1^{NCKL}$, or the empty FLAG expression vector. In HEK 293T cells, we immunoprecipitated HA-KRAS and probed for binding to endogenous BRAF and FLAG-RASSF (**Fig 9**). As expected, endogenous BRAF showed increased binding to the constitutively active (G12V) KRAS mutants compared to wild-type KRAS. Additionally, BRAF showed reduced binding with $KRAS^{G12V/I21F/H27R}$ compared to $KRAS^{G12V}$. Conversely, RASSF5 and $RASSF1^{NCKL}$ showed increased binding with $KRAS^{G12V/I21F/H27R}$ compared to $KRAS^{G12V}$. No binding was observed between KRAS and $RASSF1^{WT}$, consistent with our earlier data. These results confirmed that the binding preferences of the KRAS and RASSF1 rewiring mutants observed *in vitro* were also observed in cells, and we could therefore use these designed mutants in BioID experiments.

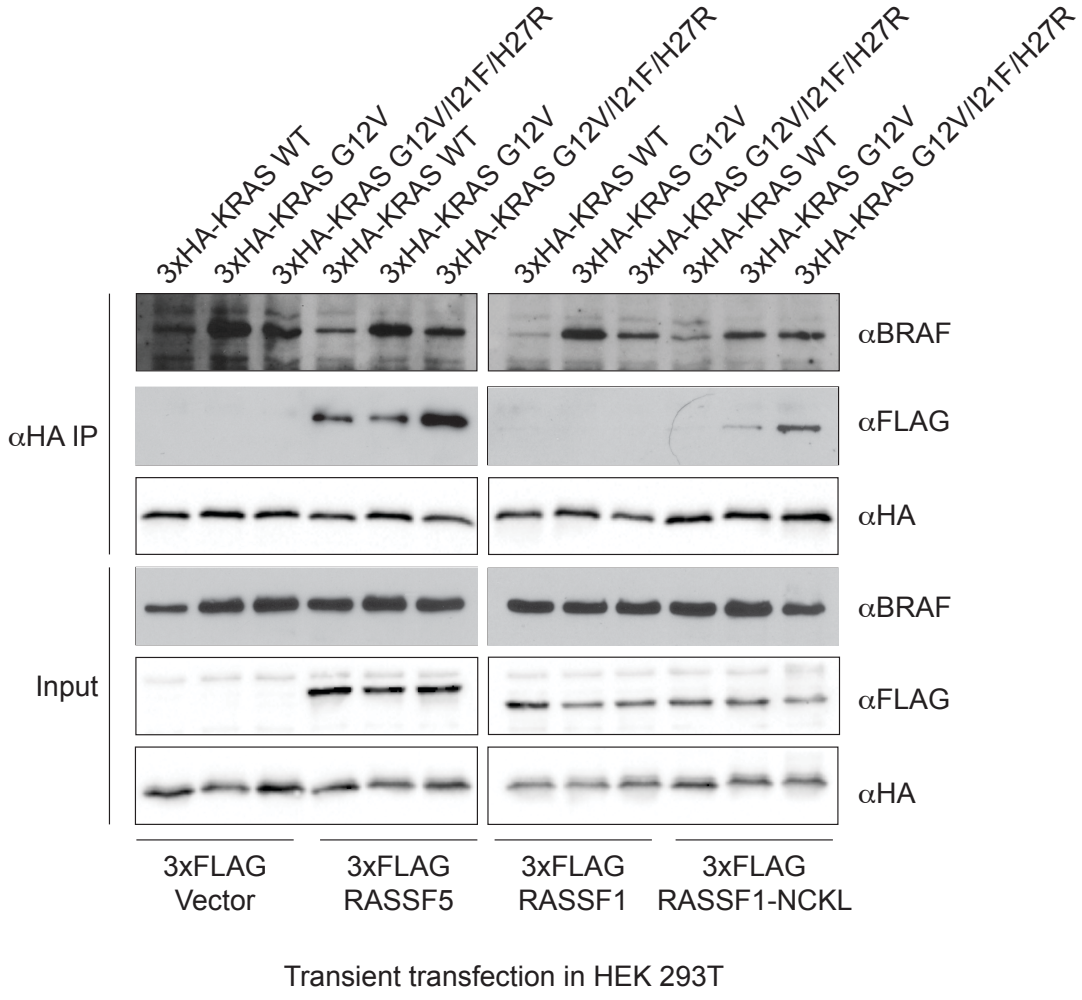

Figure 9. KRAS$^{G12V/I21F/H27R}$ has increased affinity for RASSF5 and decreased affinity for BRAF in cells

HEK 293T cells were transiently co-transfected with 3xHA-tagged KRAS and 3xFLAG-tagged RASSF1, RASSF1$^{N149C/K208L}$, RASSF5, or an empty 3xFLAG vector. Subsequently, an immunoprecipitation (IP) with anti-HA antibody was performed. Immunoblots were probed with anti-FLAG and anti-BRAF antibodies to assess the binding of the different KRAS mutants with the RASSF proteins and with endogenous BRAF.

Generation of stable cell lines for BioID

With the aim of identifying proteins that play a role in the activation of the Hippo pathway downstream of KRAS, we set out to perform a series of BioID experiments to map the interactomes of KRAS and RASSF1/5, either alone or when co-expressed.

We subcloned genes encoding full length RASSF1, RASSF5, RASSF1^{NCKL}, KRAS^{WT}, KRAS^{G12V}, KRAS$^{G12V/I21F/H27R}$, and a control (GFP) into the N-pSTV6 vector. This lentiviral vector comprises a BirA*-FLAG tag under control of a doxycycline-inducible promoter where expression of a BirA*-FLAG-bait fusion protein is induced upon addition of doxycycline to the media, allowing for control of the timing and duration of expression (123).

Prior to generating stable U2OS lines, we verified expression of the BirA*-FLAG tagged baits in HEK 293T cells upon addition of doxycycline (**Fig 10A**) and confirmed the total amount of biotinylated proteins in cells increases upon expression of each BirA*-FLAG-Bait recombinant protein (**Fig 10B**). This validated the activity of the BirA* enzyme fused to our baits of interests. We further checked whether a known interactor of a given bait could be biotinylated upon its expression. To accomplish this, HEK 293T cells were co-transfected with the BirA*-FLAG-Bait constructs for RASSF1, RASSF5, or GFP alone together with HA-tagged KRAS^{WT}, KRAS^{G12V}, or KRAS$^{G12V/I21F/H27R}$ in the presence of doxycycline and biotin. We immunoprecipitated the HA-KRAS preys and probed with streptavidin-HRP to assess whether KRAS was biotinylated. This demonstrated that KRAS^{G12V} and KRAS$^{G12V/I21F/H27R}$ are biotinylated when BirA*-FLAG-RASSF5 is expressed, but not when BirA*-FLAG-GFP or BirA*-FLAG-RASSF1 are expressed (**Fig 10C**), consistent with their presumed functions. Thus, the BirA*-FLAG baits are well-expressed in mammalian cells and their expression leads to specific biotinylation of protein interactors.

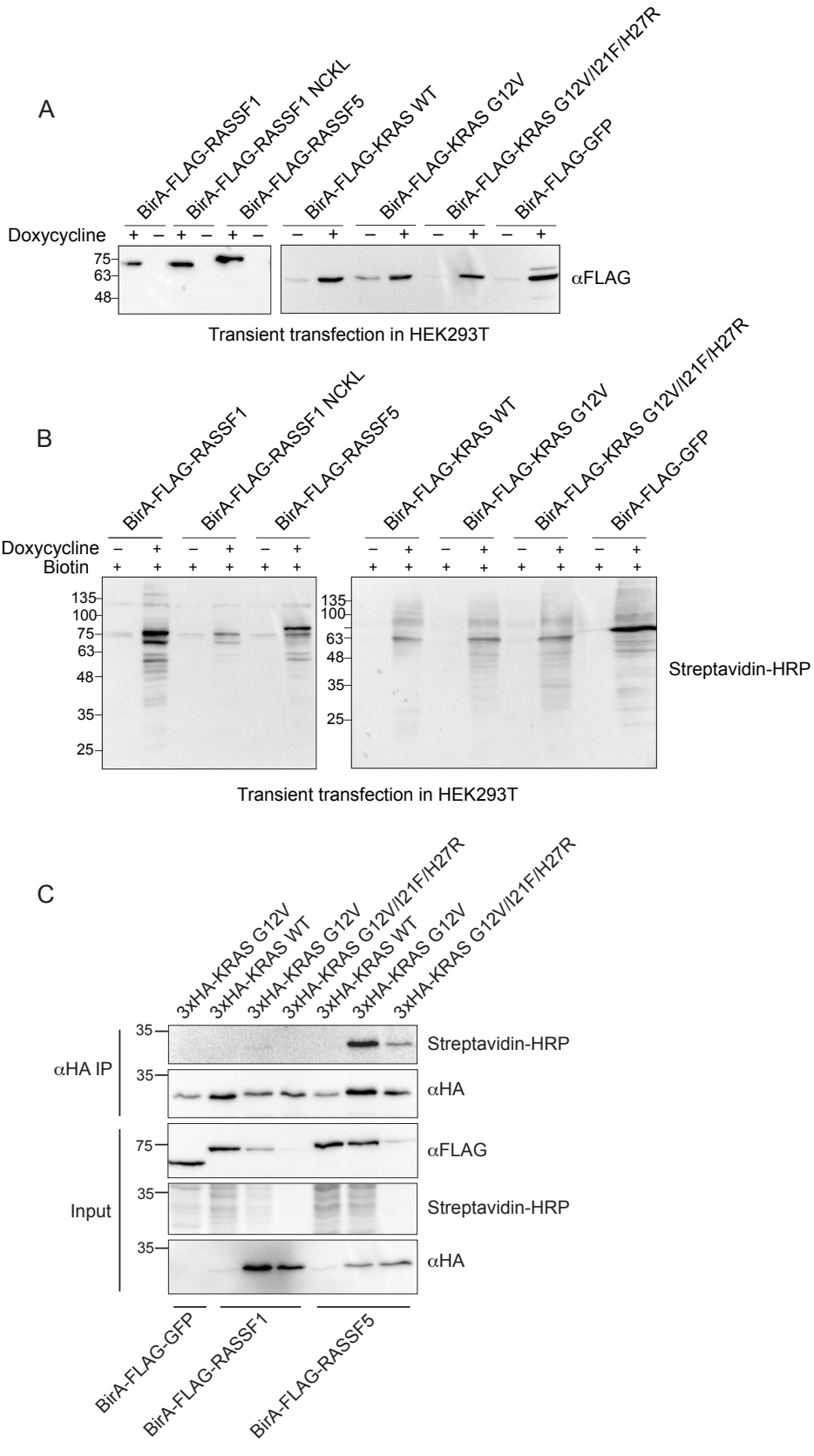
A
BirA-FLAG-RASSF1
BirA-FLAG-RASSF1 NCKL
BirA-FLAG-RASSF5
BirA-FLAG-KRAS WT
BirA-FLAG-KRAS G12V
BirA-FLAG-KRAS G12V/I21F/H27R
BirA-FLAG-GFP
Doxycycline
75
63
48
αFLAG
Transient transfection in HEK293T
B
BirA-FLAG-RASSF1
BirA-FLAG-RASSF1 NCKL
BirA-FLAG-RASSF5
BirA-FLAG-KRAS WT
BirA-FLAG-KRAS G12V
BirA-FLAG-KRAS G12V/I21F/H27R
BirA-FLAG-GFP
Doxycycline
Biotin
135
100
75
63
48
35
25
Streptavidin-HRP
Transient transfection in HEK293T
C
3xHA-KRAS G12V
3xHA-KRAS WT
3xHA-KRAS G12V
3xHA-KRAS G12V/I21F/H27R
3xHA-KRAS WT
3xHA-KRAS G12V
3xHA-KRAS G12V/I21F/H27R
αHA IP
Streptavidin-HRP
αHA
Input
αFLAG
Streptavidin-HRP
αHA
BirA-FLAG-GFP
BirA-FLAG-RASSF1
BirA-FLAG-RASSF5
Transient transfection in HEK293T

Figure 10. Validation of the BirA*-FLAG baits in HEK 293T cells

(A) All 6 constructs used for BioID as well as the GFP control were transiently transfected in HEK 293T cells. The expression of each recombinant protein in presence or absence of doxycycline was assessed by immunoblot with anti-FLAG antibody. (B) The 6 BirA*-FLAG tagged baits and GFP control were transiently transfected in HEK 293T cells, and biotin and doxycycline were added to the media. The presence of biotinylated proteins in each lysate was assessed by probing with streptavidin-HRP. (C) An IP was performed to assess whether cells expressing BirA*-FLAG-GFP, BirA*-FLAG-RASSF1 or BirA*-FLAG-RASSF5 have a capacity to biotinylate 3xHA-tagged KRAS. HEK 293T cells were co-transfected with the BirA*-FLAG tagged baits and with 3xHA-tagged KRAS mutants. Subsequently, an IP with anti-HA antibody was performed and blots were probed with streptavidin-HRP to assess biotinylation. Expression of BirA*-FLAG constructs was uneven between samples and this experiment must be repeated, but clearly demonstrates that RASSF5 is proximal to KRAS in cells.

We chose to perform the BioID in U2OS osteosarcoma cells since Hippo pathway function is intact in this cell line as we're able to observe regulation of YAP's subcellular localization (88). Using lentiviral infection, we made stable doxycycline-inducible U2OS cell lines expressing each of the BirA*-FLAG-bait recombinant proteins. As is the case in many cancer cell lines, the tumour suppressors RASSF1 and RASSF5 are significantly downregulated in osteosarcomas (124–126). In the context of this study, we considered the low expression of the RASSF proteins in U2OS cells as an advantage since it allowed us to compare between conditions where RASSF proteins were overexpressed versus those where the RASSF proteins were not expressed.

We began by performing six BioIDs where the bait was the only protein overexpressed (**Table 4**). A control run was performed using BirA*-FLAG-GFP as bait to assess non-specific biotinylation of intracellular proteins. Wild-type U2OS cells grown in the presence of biotin were used as a control for endogenous biotinylation. For all six of these BioIDs, our previous data suggest the Hippo pathway is inactive as we are overexpressing only a RASSF protein or KRAS alone, rather than both together (**Fig 4**).

Given that the aim of this study was to uncover factors involved in the RAS-mediated activation of the Hippo pathway, it was necessary to compare between the Hippo-active and -inactive conditions. Thus, we performed five combination BioIDs representing the Hippo-active conditions (**Table 4**). In these five experiments, the bait was co-expressed with a second protein such that both a RASSF effector (RASSF1 or RASSF5) and constitutively active KRAS ($KRAS^{G12V}$ or $KRAS^{G12V/I21F/H27R}$) were present.

Table 4: List of BioID experiments performed

Bait	Control
Individual BioIDs	
1. $KRAS^{WT}$ 2. $KRAS^{G12V}$ 3. $KRAS^{G12V/I21F/H27R}$ 4. RASSF1 5. $RASSF1^{NCKL}$ 6. RASSF5	GFP
Combination BioIDs	
7. $KRAS^{G12V}$ with RASSF5	GFP with RASSF5
8. $KRAS^{G12V/I21F/H27R}$ with RASSF5	
9. RASSF1 with $KRAS^{G12V}$	GFP with $KRAS^{G12V}$
10. RASSF5 with $KRAS^{G12V}$	
11. RASSF5 with $KRAS^{G12V/I21F/H27R}$	GFP with $KRAS^{G12V/ I21F/H27R}$

To generate stable U2OS cell lines where expression of both proteins is under the inducible control of doxycycline, we used the Flp-In T-REx system combined with lentiviral infection of the BirA*-FLAG baits. The Flp-In T-REx system relies on DNA recombination by Flp recombinase at FRT sites for generation of stable mammalian cells that express a protein of interest under the control of a doxycycline-inducible promoter. First, we made Flp-In T-REx U2OS cell lines stably expressing either FLAG-tagged $KRAS^{G12V}$, $KRAS^{G12V/I21F/H27R}$, or RASSF5. Next, using the BirA*-FLAG tagged baits described above, we transduced the Flp-In T-REx U2OS cells with lentivirus to generate cell lines expressing the BirA*-FLAG-Bait protein together with the concomitant FLAG-tagged protein. Three control lines were made that express BirA*-FLAG-GFP with FLAG-tagged $KRAS^{G12V}$, $KRAS^{G12V/I21F/H27R}$, or RASSF5. Thus, we generated a total of eleven U2OS lines for BioID, as well as four control lines.

To assess the expression of the exogenously expressed constructs in all of our stable U2OS cell lines, we induced each line with doxycycline and probed for FLAG (**Fig 11**). Despite being under the control of a doxycycline-inducible promoter, we observed that in the Flp-In T-REx lines, the FLAG-tagged proteins were expressed even in the absence of doxycycline (**Fig 11B**). As this

would ensure the presence of our Hippo activating prey upon doxycycline induction of the BirA*-FLAG-bait, we reasoned that it was actually advantageous to have only the BioID protein be fully inducible. Initial analysis of BirA*-FLAG-RASSF5 expression in the two lines where FLAG-tagged $KRAS^{G12V}$ or $KRAS^{G12V/I21F/H27R}$ were expressed, showed very low expression levels (**Fig 11B**). Thus, we remade these two lines using twice as much viral titre to increase expression of BirA*-FLAG-RASSF5. For the BioID, we used the old lines for the first biological replicate and the new lines for the second biological replicate. Thus, all BirA*-FLAG baits and concomitant FLAG-tagged proteins were well expressed in the fifteen stable U2OS lines and were ready for BioID.

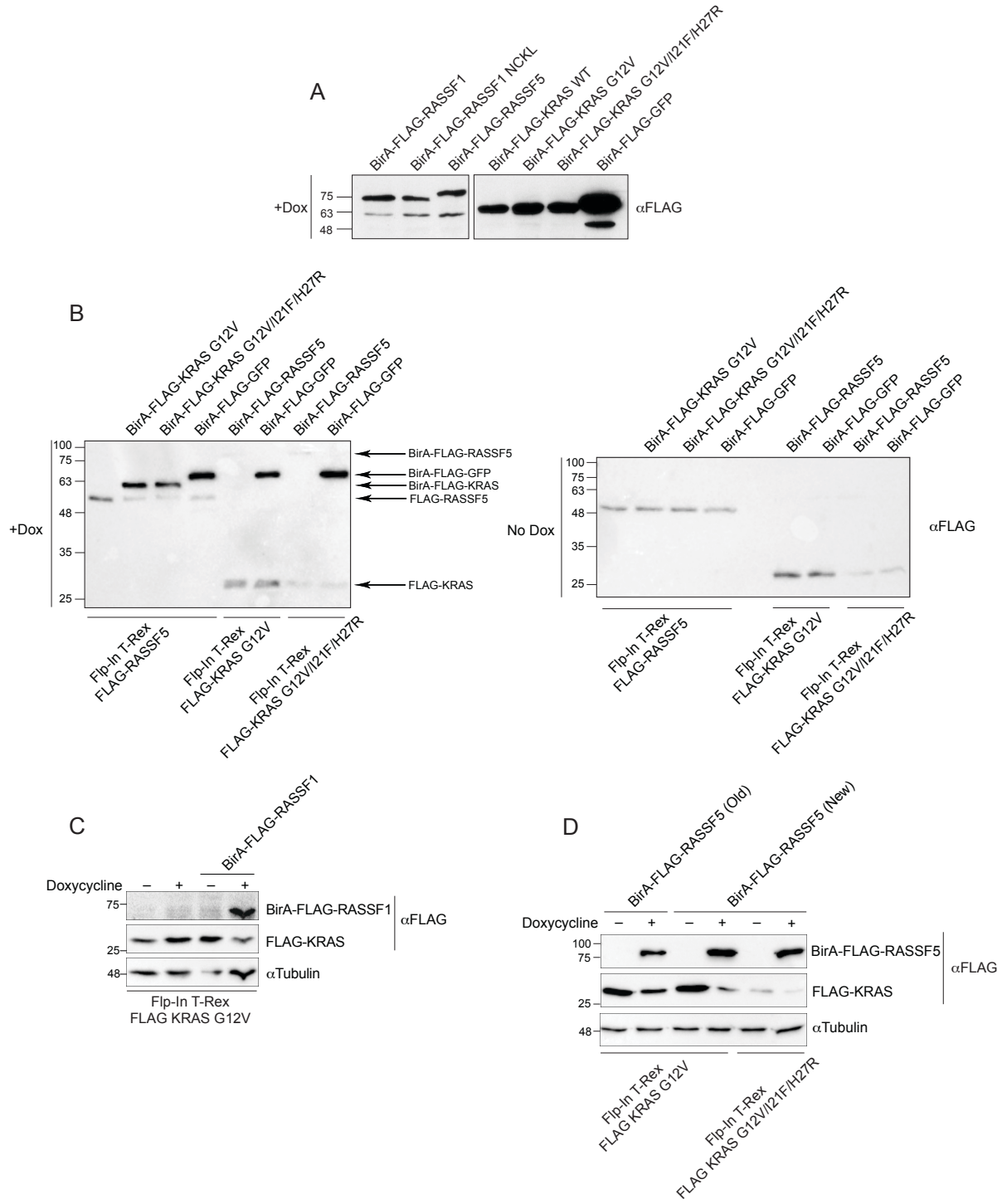

Figure 11. Expression of BirA*-FLAG-baits in stable U2OS cell lines

(A) Lentiviral infection of the BirA*-FLAG constructs in U2OS cells, followed by selection with puromycin was performed to generate stable cell lines. Expression of the BioID recombinant proteins following addition of doxycycline was assessed by immunoblot with anti-FLAG antibody. (B) (C) Stable Flp-In T-REx U2OS lines expressing either FLAG-RASSF5, FLAG-KRAS^{G12V} or

FLAG-KRAS$^{G12V/I21F/H27R}$ were generated. These lines were subsequently infected with one of the BirA*-FLAG-bait constructs to generate lines where both the BioID recombinant protein and a second FLAG-tagged protein are expressed upon addition of doxycycline. Expression of both proteins was assessed by immunoblot with anti-FLAG antibody. (D) Expression of BirA*-FLAG-RASSF5 was poor in two of the generated lines in (B), thus lentiviral infection was repeated using double the initial viral titre. Expression of both proteins was assessed by immunoblot with anti-FLAG antibody.

Validation of the correct function of the BirA*-FLAG baits in the BioID lines

To determine whether the BirA*-FLAG baits were indeed biotinylating known interaction partners in the U2OS lines, we examined whether known KRAS effectors were biotinylated in the BirA*-FLAG-KRAS lines, by immunoprecipitating (IP) the prey and probing with streptavidin-HRP. We refer to this type of experiment as a biotinylation-IP. The first biotinylation-IP we performed was to assess whether RASSF5 is biotinylated by BirA*-FLAG-KRAS. We overexpressed Venus-tagged RASSF5 in the three BioID lines expressing either BirA*-FLAG-KRAS^{WT}, BirA*-FLAG-KRAS^{G12V}, or BirA*-FLAG-KRAS$^{G12V/I21F/H27R}$. Subsequently, we immunoprecipitated Venus-RASSF5 and probed the blot with streptavidin-HRP and anti-FLAG antibody. We observed that constitutively active KRAS was complexed with RASSF5 and that RASSF5 was biotinylated in the cell lines where constitutively active KRAS was expressed (**Fig 12A**). This showed that the BirA*-FLAG baits work reliably in the stable U2OS lines and that the biotinylation-IP strategy could be used for hit validation.

Next, we assessed whether the effector RAF1 was biotinylated by BirA*-FLAG-KRAS. Using the five KRAS BioID cell lines, we immunoprecipitated endogenous RAF1 and probed the blot with streptavidin-HRP and anti-FLAG antibody. RAF1 was most strongly biotinylated in the two samples expressing BirA*-FLAG-KRAS^{G12V}. RAF1 was also biotinylated to a smaller extent in the sample expressing BirA*-FLAG-KRAS$^{G12V/I21F/H27R}$ alone, and to an even smaller extent in the sample expressing BirA*-FLAG-KRAS$^{G12V/I21F/H27R}$ with RASSF5, presumably because RASSF5 was outcompeting RAF1 for binding to KRAS$^{G12V/I21F/H27R}$ (**Fig 12B**). Thus, we showed that known KRAS interactors were subject to biotinylation in the BioID lines, confirming the correct function of the BirA*-FLAG baits.

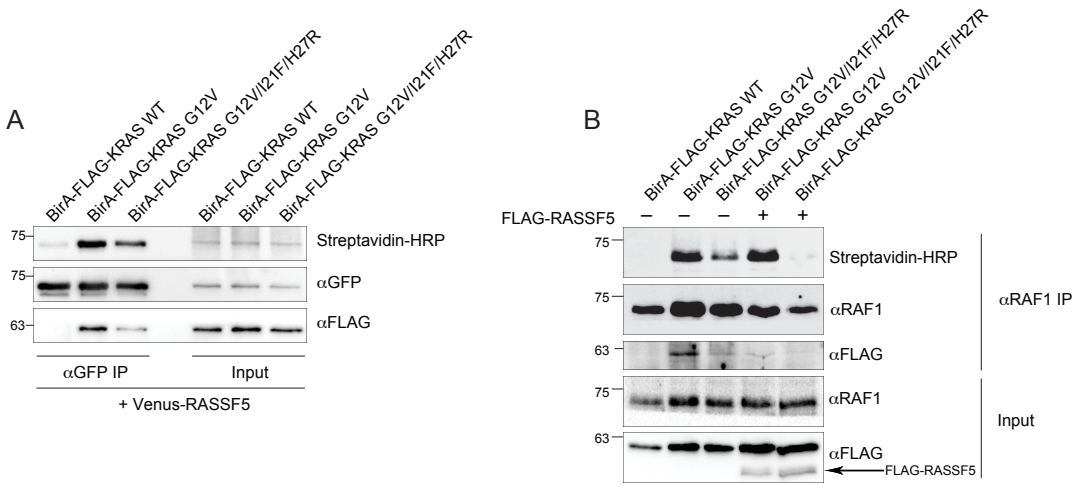

Figure 12. Biotinylation of KRAS interactors in the KRAS BioID lines

(A) Venus-RASSF5 was transiently transfected in the BioID U2OS cell lines expressing BirA*-FLAG tagged $KRAS^{WT}$, $KRAS^{G12V}$ or $KRAS^{G12V/I21F/H27R}$ and doxycycline and biotin were added to the media. Subsequently, an IP with anti-GFP antibody was performed and blots were probed with streptavidin-HRP to assess whether RASSF5 is biotinylated. (B) Doxycycline and biotin were added to the media of the 5 KRAS BioID U2OS cell lines. Subsequently, an IP with anti-RAF1 antibody was performed, and the blots were probed with streptavidin-HRP to assess whether endogenous RAF1 is biotinylated.

The BioID Results

Having validated the function of the BirA*-FLAG baits in the stable U2OS lines, we proceeded with performing BioID proximity biotinylation. Expression of the BirA*-FLAG-Bait fusion protein was induced with doxycycline and the cells were incubated with biotin for 24 hours. Subsequently, all biotinylated proteins in the cell lysate in were purified on streptavidin beads. Virtually all biotinylated proteins in the cell lysate became bound to the beads (**Fig 13**). Isolated proteins were trypsinized and identified by mass spectrometry. Two biological replicates were performed for each BioID experiment.

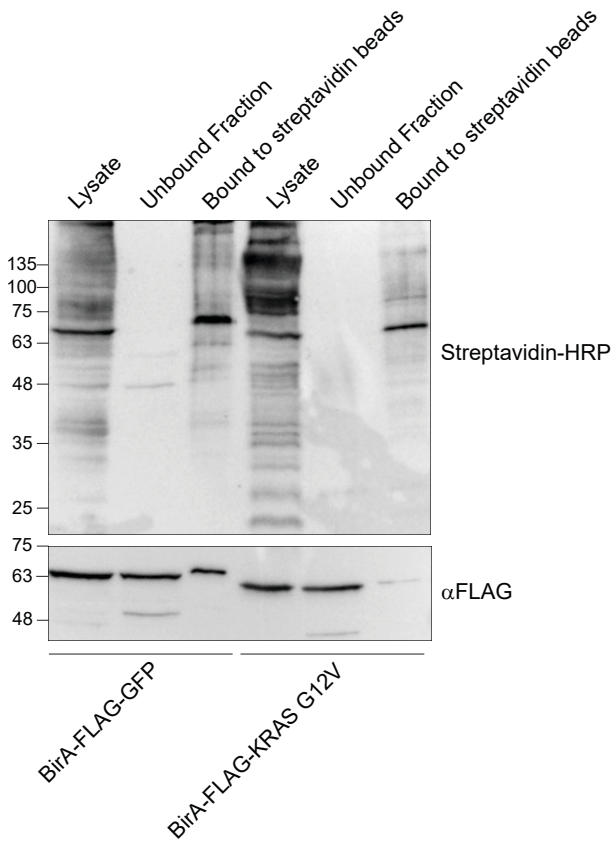

Figure 13. Purification of biotinylated proteins on streptavidin beads

The U2OS cells used for BioID were lysed and biotinylated proteins were purified on streptavidin-sepharose beads. Different fractions were probed with streptavidin. Most biotinylated proteins in the sample were bound to the beads.

The mass spectrometry results were analysed using ProHits (120), and SAINTexpress (122) was used to determine preys deemed statistically significant. For most of our analysis we only included hits with a SAINT score greater or equal to 0.9. When making figures 15, 16, and 17, we also included hits with a SAINT score greater or equal to 0.5. Given that more spectra are identified for larger proteins on average, we normalized the spectral abundance of each hit to the protein length (121). The total number of spectra identified per BioID might vary between experiments (for example, due to differences in expression of the BirA*-bait), thus comparing between datasets can be difficult. Therefore, we also normalized the spectral abundance of each hit to the total number of spectra identified per BioID experiment (121).

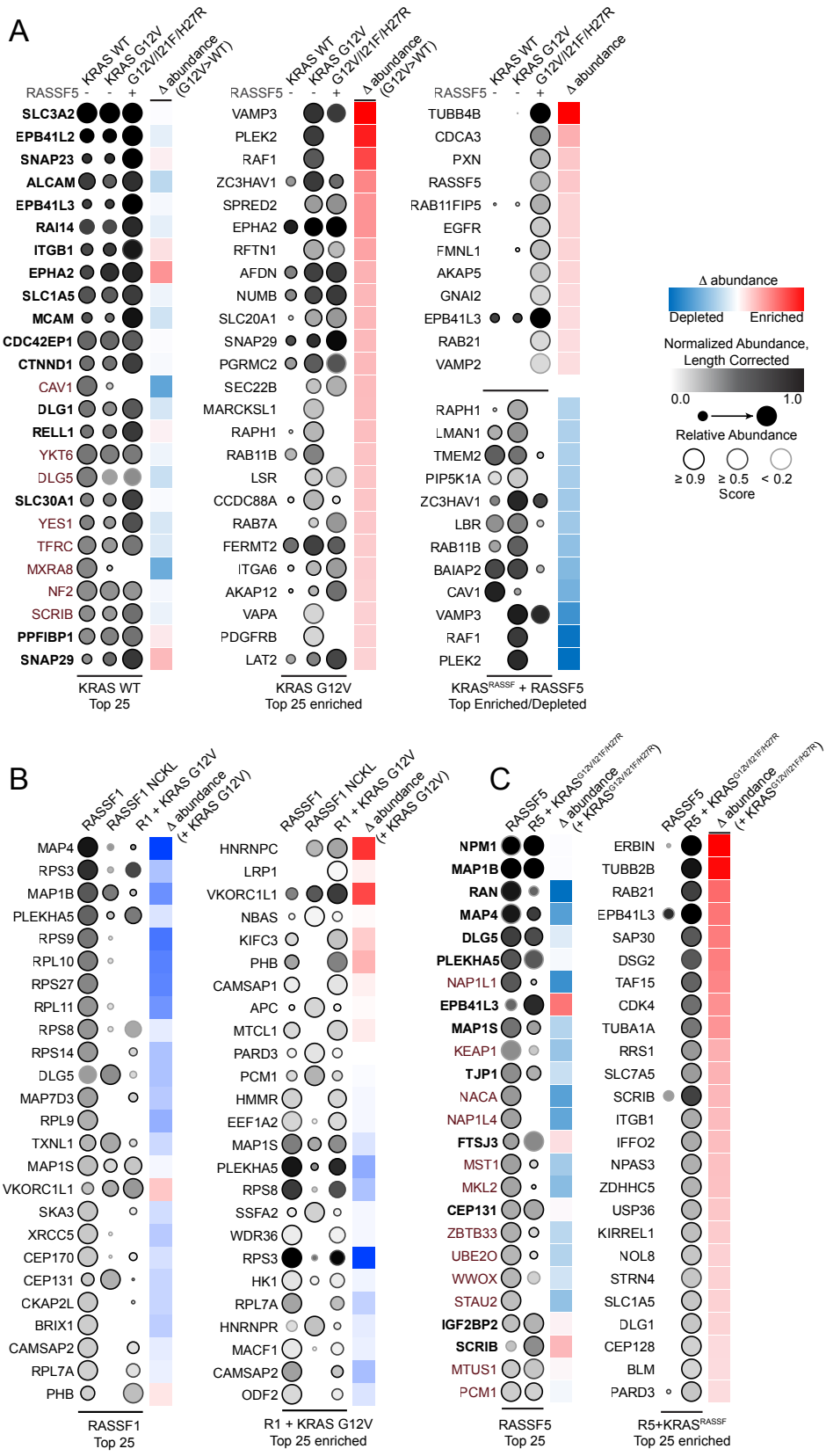
A
KRAS WT
KRAS G12V
G12V/I21F/H27R
Δ abundance (G12V>WT)
RASSF5
SLC3A2
EPB41L2
SNAP23
ALCAM
EPB41L3
RAI14
ITGB1
EPHA2
SLC1A5
MCAM
CDC42EP1
CTNND1
CAV1
DLG1
RELL1
YKT6
DLG5
SLC30A1
YES1
TFRC
MXRA8
NF2
SCRIB
PPFIBP1
SNAP29
KRAS WT Top 25
VAMP3
PLEK2
RAF1
ZC3HAV1
SPRED2
EPHA2
RFTN1
AFDN
NUMB
SLC20A1
SNAP29
PGRMC2
SEC22B
MARCKSL1
RAPH1
RAB11B
LSR
CCDC88A
RAB7A
FERMT2
ITGA6
AKAP12
VAPA
PDGFRB
LAT2
KRAS G12V Top 25 enriched
TUBB4B
CDCA3
PXN
RASSF5
RAB11FIP5
EGFR
FMNL1
AKAP5
GNAI2
EPB41L3
RAB21
VAMP2
RAPH1
LMAN1
TMEM2
PIP5K1A
ZC3HAV1
LBR
RAB11B
BAIAP2
CAV1
VAMP3
RAF1
PLEK2
KRASRASSF + RASSF5 Top Enriched/Depleted
Δ abundance
Depleted
Enriched
Normalized Abundance, Length Corrected
0.0
1.0
Relative Abundance
≥ 0.9
≥ 0.5
< 0.2
Score
B
RASSF1
RASSF1 NCKL
R1 + KRAS G12V
Δ abundance (+ KRAS G12V)
MAP4
RPS3
MAP1B
PLEKHA5
RPS9
RPL10
RPS27
RPL11
RPS8
RPS14
DLG5
MAP7D3
RPL9
TXNL1
MAP1S
VKORC1L1
SKA3
XRCC5
CEP170
CEP131
CKAP2L
BRIX1
CAMSAP2
RPL7A
PHB
RASSF1 Top 25
HNRNPC
LRP1
VKORC1L1
NBAS
KIFC3
PHB
CAMSAP1
APC
MTCL1
PARD3
PCM1
HMMR
EEF1A2
MAP1S
PLEKHA5
RPS8
SSFA2
WDR36
RPS3
HK1
RPL7A
HNRNPR
MACF1
CAMSAP2
ODF2
R1 + KRAS G12V Top 25 enriched
C
RASSF5
R5 + KRASG12V/I21F/H27R
Δ abundance (+ KRASG12V/I21F/H27R)
NPM1
MAP1B
RAN
MAP4
DLG5
PLEKHA5
NAP1L1
EPB41L3
MAP1S
KEAP1
TJP1
NACA
NAP1L4
FTSJ3
MST1
MKL2
CEP131
ZBTB33
UBE2O
WWOX
STAU2
IGF2BP2
SCRIB
MTUS1
PCM1
RASSF5 Top 25
ERBIN
TUBB2B
RAB21
EPB41L3
SAP30
DSG2
TAF15
CDK4
TUBA1A
RRS1
SLC7A5
SCRIB
ITGB1
IFFO2
NPAS3
ZDHHC5
USP36
KIRREL1
NOL8
STRN4
SLC1A5
DLG1
CEP128
BLM
PARD3
R5+KRASRASSF Top 25 enriched

Figure 14. Top 25 hits in each BioID dataset

(A) Top 25 proteins identified in the BioID dataset of RASSF1 and in that of RASSF1 with $KRAS^{G12V}$. (B) Top 25 proteins identified in the BioID of RASSF5 and in that of RASSF5 with $KRAS^{G12V/I21F/H27R}$. (C) Top 25 proteins identified in the BioID of $KRAS^{WT}$, in that of $KRAS^{G12V}$, and in that of $KRAS^{G12V/I21F/H27R}$ with RASSF5. The colour intensity of each dot is proportional to the spectral abundance of each hit normalized to protein length and to total number of spectra. The size of each dot is proportional to the hit's spectral abundance relative to its abundance in the other BioIDs. The colour of the dot's border represents its SAINT score, where a darker colour indicates a higher confidence interaction. Only hits with a SAINT score ≥ 0.9 in at least one of the BioID experiments are included. The blue/red squares indicate the difference in spectral abundance between the two indicated BioID experiments.

KRAS BioID results

We began by analyzing the hits identified in the five BioIDs of KRAS. Given the membrane localization of KRAS, the list of the top 25 hits identified in the KRAS BioIDs included many membrane-localized proteins (**Fig 14A**). Namely, the top three hits in the BioID of $KRAS^{G12V}$ were SLC3A2, EPB41L2 and EPHA2, all three of which are transmembrane proteins. EPB41L2 and EPHA2 have been identified in previous BioIDs of KRAS as well (117,127,128). Thus, we felt confident that the BirA*-FLAG-KRAS proteins were properly localized at the plasma membrane.

Many known interactors of KRAS were identified among the hits, including effectors and regulators (**Fig 15**). RAS GAPs were among the interactors, including NF1 and RASAL2. However, no RAS GEFs were identified. Notably, all three RAF isoforms were identified and so was the effector AFDN. Furthermore, the RAS effectors were more highly enriched in the conditions of constitutively active KRAS ($KRAS^{G12V}$ or $KRAS^{G12V/I21F/H27R}$) than in the $KRAS^{WT}$ condition, further confirming that BioID worked reliably and that signaling downstream of BirA*-FLAG-KRAS was occurring. Interestingly, RASSF5 was identified only in the BioID of $KRAS^{G12V/I21F/H27R}$ with RASSF5. This was not unexpected in the BioIDs of KRAS alone given the low endogenous expression of RASSF5 in U2OS cells. In fact, RASSF5 has never been identified in previous BioIDs of K/H/NRAS (129). However, RASSF5 was not detected in the BioID of $KRAS^{G12V}$ with co-expressed RASSF5. This might simply be because it was not picked up by the mass spectrometry, given that we could detect the interaction by biotinylation-IP (**Fig 12A**).

The top hit enriched in the interactome of $KRAS^{G12V/I21F/H27R}$ with RASSF5 compared to that of $KRAS^{G12V}$ alone was β-tubulin 4B (TUBB4B), hinting at a possible involvement of microtubules in Hippo pathway activation. To our knowledge this is the first time tubulin has been identified as a proximal interactor of RAS.

We sought to determine which gene ontology (GO) terms for biological function (BF), cellular component (CC), and molecular function (MF) were enriched among the hits in our datasets. Based on this analysis, we grouped the KRAS BioID hits into five categories; proteins involved in GTPase signaling, protein kinases, proteins involved in cell adhesion and polarity, proteins linked to the MAPK pathway, and proteins involved in vesicular transport (**Fig 15**). Some hits did not fit any of the categories and some hits were present in two or more of these categories. Strikingly, many proteins involved in adhesion and polarity such as Erbin, SCRIB and AFDN were also present in the interactome of RASSF5.

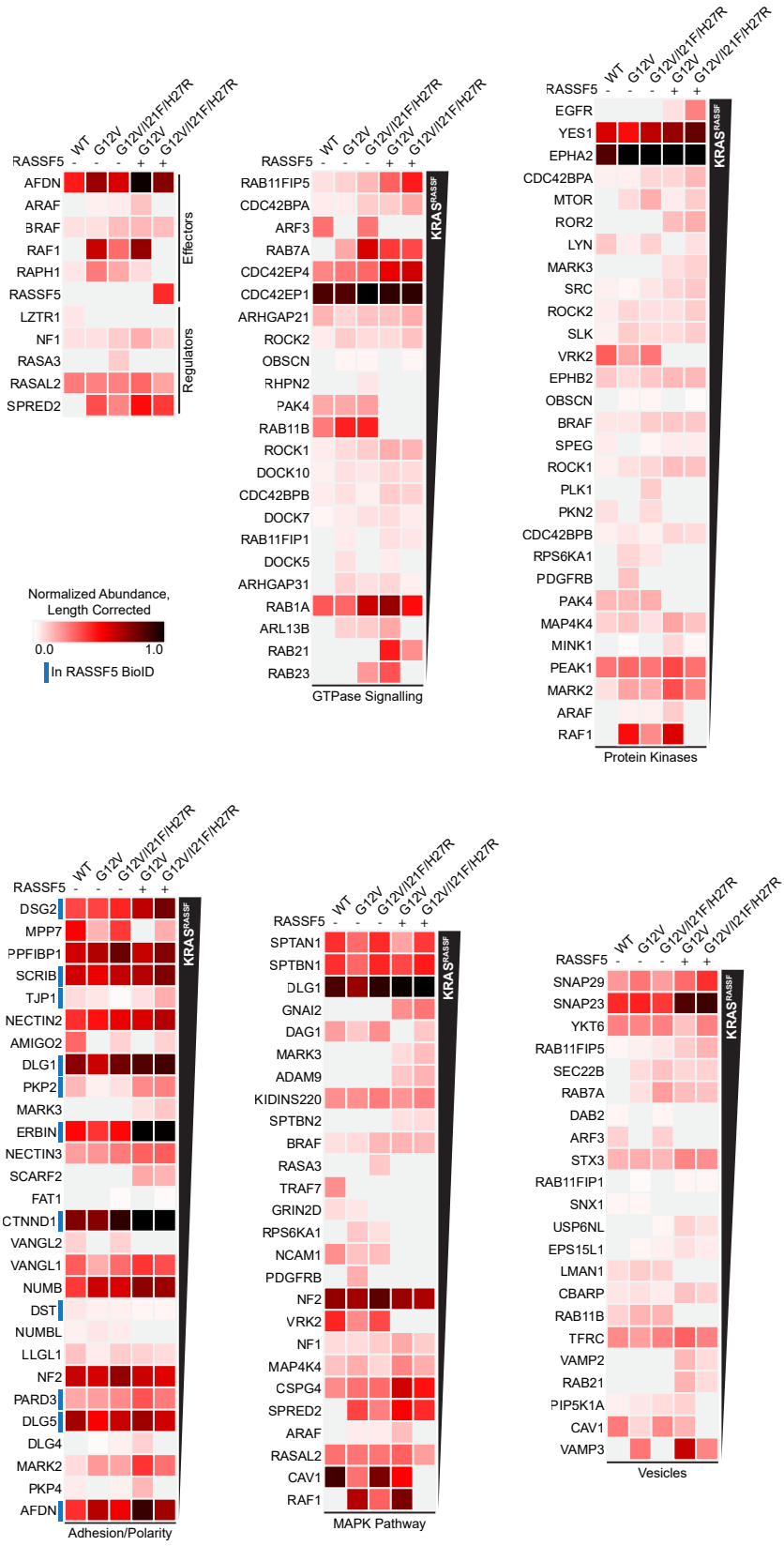
WT
G12V
G12V/I21F/H27R
G12V
G12V/I21F/H27R
RASSF5
AFDN
ARAF
BRAF
RAF1
RAPH1
RASSF5
LZTR1
NF1
RASA3
RASAL2
SPRED2
Effectors
Regulators
Normalized Abundance, Length Corrected
0.0
1.0
In RASSF5 BioID
RAB11FIP5
CDC42BPA
ARF3
RAB7A
CDC42EP4
CDC42EP1
ARHGAP21
ROCK2
OBSCN
RHPN2
PAK4
RAB11B
ROCK1
DOCK10
CDC42BPB
DOCK7
RAB11FIP1
DOCK5
ARHGAP31
RAB1A
ARL13B
RAB21
RAB23
KRASRASSF
GTPase Signalling
EGFR
YES1
EPHA2
CDC42BPA
MTOR
ROR2
LYN
MARK3
SRC
ROCK2
SLK
VRK2
EPHB2
OBSCN
BRAF
SPEG
ROCK1
PLK1
PKN2
CDC42BPB
RPS6KA1
PDGFRB
PAK4
MAP4K4
MINK1
PEAK1
MARK2
ARAF
RAF1
Protein Kinases
DSG2
MPP7
PPFIBP1
SCRIB
TJP1
NECTIN2
AMIGO2
DLG1
PKP2
MARK3
ERBIN
NECTIN3
SCARF2
FAT1
CTNND1
VANGL2
VANGL1
NUMB
DST
NUMBL
LLGL1
NF2
PARD3
DLG5
DLG4
MARK2
PKP4
AFDN
Adhesion/Polarity
SPTAN1
SPTBN1
DLG1
GNAI2
DAG1
MARK3
ADAM9
KIDINS220
SPTBN2
BRAF
RASA3
TRAF7
GRIN2D
RPS6KA1
NCAM1
PDGFRB
NF2
VRK2
NF1
MAP4K4
CSPG4
SPRED2
ARAF
RASAL2
CAV1
RAF1
MAPK Pathway
SNAP29
SNAP23
YKT6
RAB11FIP5
SEC22B
RAB7A
DAB2
ARF3
STX3
RAB11FIP1
SNX1
USP6NL
EPS15L1
LMAN1
CBARP
RAB11B
TFRC
VAMP2
RAB21
PIP5K1A
CAV1
VAMP3
Vesicles

Figure 15. Heat map representation of the KRAS BioID hits grouped by function

Heat map representation of the proteins identified in the 5 BioIDs of KRAS, grouped by cellular or molecular function: GTPase signaling, protein kinases, cell adhesion and polarity, MAPK signaling, and vesicular transport. The functional groupings were chosen by identifying gene ontology (GO) terms that were most enriched in the dataset. The colour intensity of each square is proportional to the spectral abundance of each hit normalized to protein length and to total number of spectra. Only hits with a SAINT score ≥ 0.5 in at least one of the BioID experiments are included. Hits are ordered based on the difference in spectral abundance between the BioID of $KRAS^{G12V}$ and the BioID of $KRAS^{G12V/I21F/H27R}$, i.e., hits more enriched in the BioID of $KRAS^{G12V/I21F/H27R}$ are higher up. A blue line indicates hits that were also identified in the BioID of RASSF5.

RASSF1 BioID results

The BioID of RASSF1 alone was highly enriched in ribosomal proteins (e.g., RPS3, RPS9, RPL10). These are likely non-specific interactions that failed to be filtered out by the SAINT algorithm, resulting from the ribosomal synthesis of the BirA*-bait recombinant protein (130).

Many microtubule-associated proteins (MAPs) such as MAP4, MAP1S, and MAP1B were enriched in the BioID of RASSF1 alone and in that of RASSF1 with $KRAS^{G12V}$, consistent with RASSF1's observed localization at microtubules (104). Despite our previous data showing that the $RASSF1^{NCKL}$ mutant does not localize at microtubules, many MAPs were identified in the interactome of $KRAS^{NCKL}$, although fewer than in the two $RASSF1^{WT}$ BioIDs (**Fig 16**). The interactome of $RASSF1^{NCKL}$ was more highly enriched in cell adhesion and polarity proteins compared to that of $RASSF1^{WT}$, although it is interesting to note that $RASSF1^{WT}$ was nonetheless in proximity to some cell adhesion proteins, despite its microtubule localization. Qualitatively, the interactome of RASSF1 alone more closely resembles that of RASSF1 with $KRAS^{G12V}$ than that of $RASSF1^{NCKL}$.

When $KRAS^{G12V}$ was expressed, most hits were depleted rather than enriched (**Fig 14B**). Such hits include MAP4, MAP1B and the Hippo pathway inhibitor DLG5. Two hits that were markedly enriched in the BioID of RASSF1 with $KRAS^{G12V}$ are the RNA-binding protein HNRNPC and the lipoprotein receptor LRP1. TUBB4B and α-tubulin 1C (TUBA1C) were also among the enriched hits.

Prey interactors that were enriched in the BioID of $RASSF1^{NCKL}$ compared to that of $RASSF1^{WT}$ include HNRNPC, the mRNA-binding protein IGF2BP2, and centrosomal proteins

CEP128 and CEP131, whereas depleted proteins include MAP4, MAP7D3, and the mitotic-spindle associated protein SKA3.

In addition to DLG5, several other Hippo pathway regulators were identified in the RASSF1 BioIDs. Notably, NF2, which is PM-localized, was only observed as a hit for RASSF1^{NCKL}. The kinases MST1 and MST2, known interactors of RASSF1, were identified in all three RASSF1 interactomes, although they were both significantly depleted in the BioID of RASSF1 with KRAS^{G12V}.

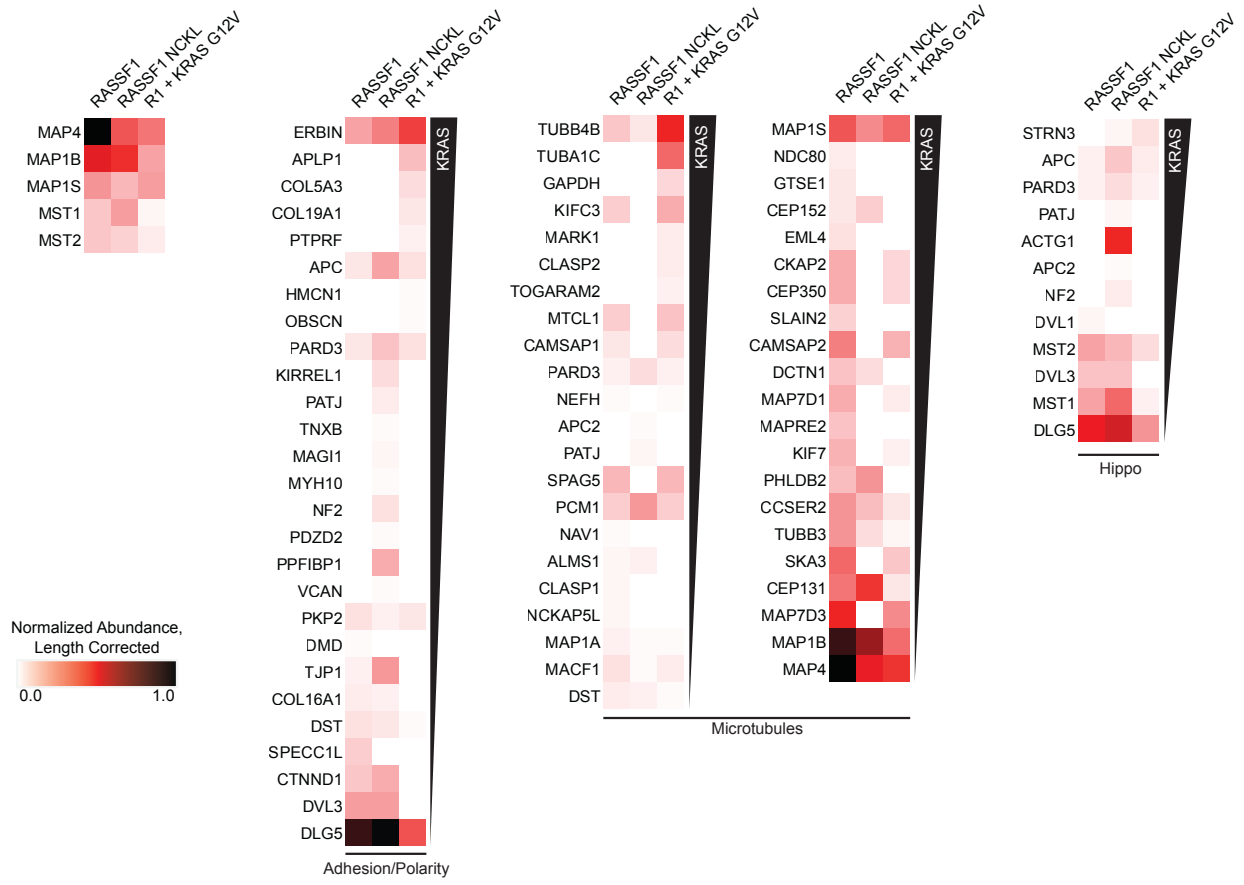

Figure 16. Heat map representation of the RASSF1 BioID hits grouped by function

Heat map representation of the proteins identified in the 3 BioIDs of RASSF1, grouped by cellular or molecular function: cell adhesion and polarity, association with microtubules, and Hippo signaling. The functional groupings were chosen by identifying GO terms that were most enriched in the dataset. The colour intensity of each square is proportional to the spectral abundance of each hit normalized to protein length and to total number of spectra. Only hits with a SAINT score ≥ 0.5 in at least one of the BioID experiments are included. Hits are ordered based on the difference

in spectral abundance between the BioID of RASSF1 and that of RASSF1 with $KRAS^{G12V}$, i.e., hits more enriched in the BioID of RASSF1 with $KRAS^{G12V}$ are higher up.

RASSF5 BioID results

RASSF5 has been shown to have primarily nuclear localization. Consistent with this, many of the RASSF5 BioID hits were nuclear proteins such as Nucleophosmin (NPM1), which was the top hit (**Fig 14C**). The third top interactor for RASSF5 was the small GTPase RAN, which mediates nuclear import and export of proteins, likely indicative of nucleocytoplasmic shuttling of RASSF5. Notably NPM1, RAN, as well as other nuclear proteins such as the nucleosome assembly proteins NAP1L1 and NAP1L4 were highly depleted when $KRAS^{G12V}$ or $KRAS^{G12V/I21F/H27R}$ were expressed. This is consistent with our observations that when constitutively active KRAS is expressed, RASSF5 colocalizes with KRAS at the PM.

Proteins that were highly enriched when $KRAS^{G12V}$ or $KRAS^{G12V/I21F/H27R}$ were expressed include the PM-localized polarity protein Erbin, desmosome-localized Desmoglein 2 (DSG2), and α-tubulin 1A (TUBA1A). Additionally, β-tubulin 2B (TUBB2B) and the small GTPase RAB21 were enriched only when $KRAS^{G12V/I21F/H27R}$ (but not $KRAS^{G12V}$) was expressed.

As with RASSF1 and $RASSF1^{NCKL}$, a significant number of MAPs were among the RASSF5 interactors, including MAP1B and MAP4, which were the second and fourth top interactors of RASSF5, respectively (**Fig 17**). The RASSF5 hits included Hippo pathway regulators such as DLG5 and SCRIB. MST1 and MST2 were identified in the interactome of RASSF5 alone, and they were significantly depleted in the interactome of RASSF5 with $KRAS^{G12V}$ and in that of RASSF5 with $KRAS^{G12V/I21F/H27R}$.

It has been demonstrated that RASSF1 and RASSF5 can heterodimerize *in vitro* through GST-pulldown experiments with purified proteins (105). RASSF1 was not identified in the BioID of RASSF5, and RASSF5 was not identified in the BioID of RASSF1 likely because they are poorly expressed in U2OS cells and because they don't share the same cellular localization. However, RASSF5 was identified as a proximal interactor of $RASSF1^{NCKL}$. $RASSF1^{NCKL}$ and RASSF5, which based on our previous observations have the same subcellular localization, might be heterodimerizing *in vivo*.

Notably, neither $KRAS^{G12V}$ nor $KRAS^{G12V/I21F/H27R}$ were detected in the BioID of RASSF5. Again, this might be because it was not detected by mass spectrometry, given that the interaction was indeed detected by biotinylation-IP in HEK 293T cells (**Fig 10C**).

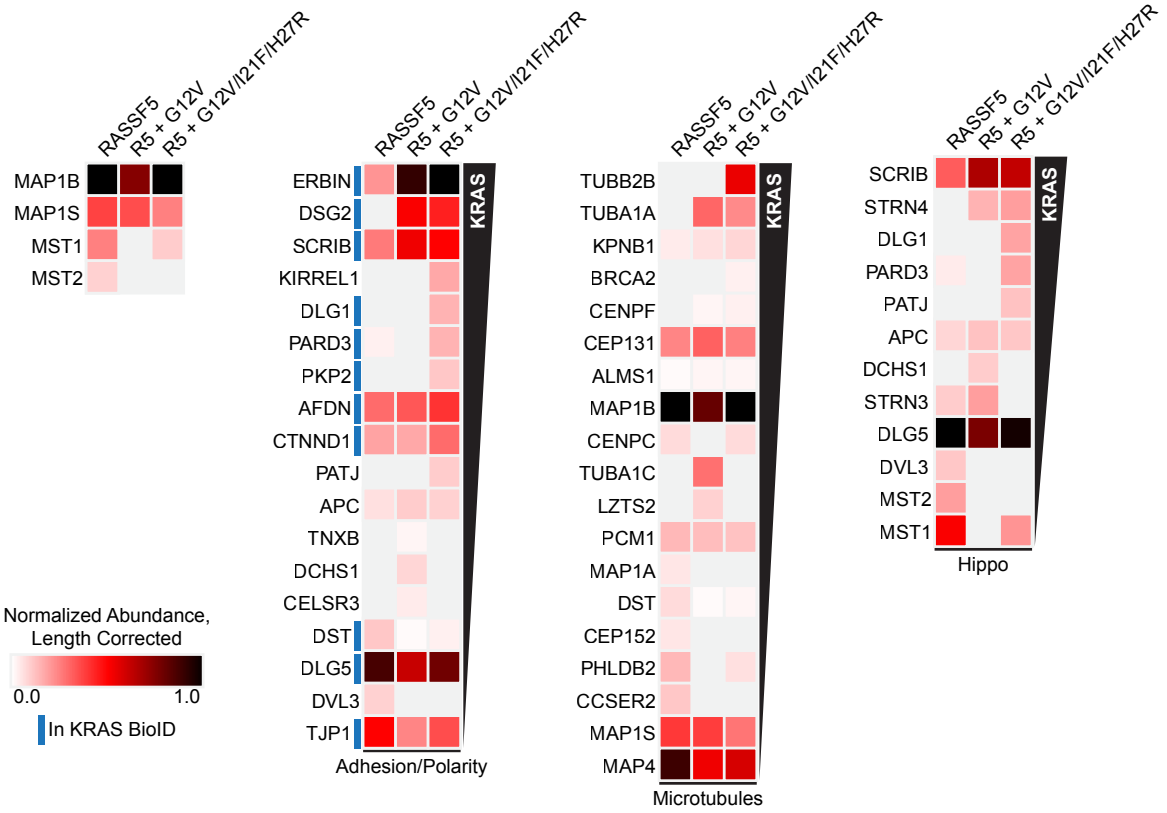

Figure 17. Heat map representation of the RASSF5 BioID hits grouped by function

Heat map representation of the proteins identified in the 3 BioIDs of RASSF5, grouped by cellular or molecular function: cell adhesion and polarity, association with microtubules, and Hippo signaling. The functional groupings were chosen by identifying gene GO terms that were most enriched in the dataset. The colour intensity of each square is proportional to the spectral abundance of each hit normalized to protein length and to total number of spectra. Only hits with a SAINT score ≥ 0.5 in at least one of the BioID experiments are included. Hits are ordered based on the difference in spectral abundance between the BioID of RASSF5 and that of RASSF5 with $KRAS^{G12V/I21F/H27R}$, i.e., hits more enriched in the BioID of RASSF5 with $KRAS^{G12V/I21F/H27R}$ are higher up. A blue line indicates hits that were also identified in the BioID of KRAS.

KRAS interaction with SNAP23 and VAMP3

We were interested in determining which BioID hits could be involved in activation of the Hippo pathway downstream of KRAS and the RASSF effectors. We found it particularly interesting that a number of proteins involved in vesicular trafficking were among the KRAS BioID hits, and furthermore, that the spectral abundance of many of these hits seemed to vary in the conditions where RASSF5 was present. This led us to hypothesize that RASSF5 or the Hippo pathway can regulate KRAS expression at the membrane by modulating its vesicular trafficking

(131). Of particular interest to us were the SNARE proteins SNAP23, SNAP29 and VAMP3. SNAREs are proteins that mediate the fusion of vesicles with target membranes (132). These three SNAREs have been shown to interact with KRAS and regulate its localization to the plasma membrane (131). Focussing on SNAP23 and VAMP3, we aimed to validate these two hits as KRAS interactors through biotinylation-IP experiments. In U2OS cells expressing either BirA*-FLAG-KRAS^{WT}, BirA*-FLAG-KRAS^{G12V}, or BirA*-FLAG-KRAS^{G12V} with RASSF5, we transiently expressed either HA-SNAP23 or HA-VAMP3, and subsequently immunoprecipitated the HA-tagged SNARE protein and probed with streptavidin-HRP to assess whether it was biotinylated (**Fig 18**). We observed that both SNAP23 and VAMP3 were biotinylated when BirA*-FLAG-KRAS was expressed, however, the amount of biotinylation did not vary when RASSF5 was expressed, in contrast to what we observed in the BioID data. Thus, we successfully validated that SNAP23 and VAMP3 as proximal interactors of KRAS.

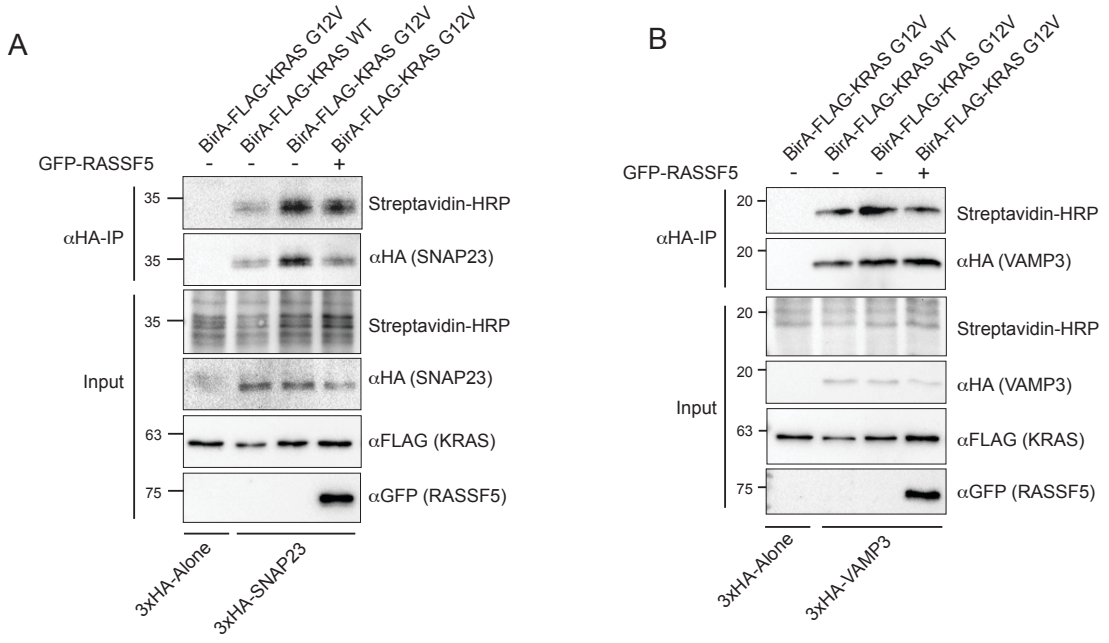

Figure 18. SNAP23 and VAMP3 are biotinylated by BirA*-FLAG-KRAS

(C) BioID U2OS cell lines expressing either BirA*-FLAG-KRAS^{WT} or BirA*-FLAG-KRAS^{G12V} were used for this IP. Using lentiviral infection, GFP-RASSF5 was expressed in one of the samples expressing BirA*-FLAG-KRAS^{G12V}. 3xHA-tagged SNAP23 or the empty 3xHA vector were transiently transfected, and doxycycline and biotin were added to the media. Subsequently, an IP

with anti-HA antibody was performed, and the blots were probed with streptavidin-HRP to assess whether SNAP23 is biotinylated. (D) Same experiment as in (C) but 3xHA-tagged VAMP3 was transiently transfected instead.

DISCUSSION

A summary of the findings

RAS can engage several effectors to activate a multitude of downstream pathways. How RAS might select effectors to engage and thus which pathways to activate is not fully understood. This versatility and crosstalk between pathways make it difficult to study RAS signaling to a single effector pathway. Rewiring of RAS by point mutations is a useful tool to study RAS signaling downstream of a specific effector. Compared to wild-type KRAS, the $KRAS^{I21F/H27R}$ double mutant had increased affinity for RASSF5 and decreased affinity for RAF *in vitro* and in cells. Endogenous BRAF displayed less binding to $KRAS^{G12V/I21F/H27R}$ compared to $KRAS^{G12V}$, whereas exogenously expressed RASSF5 displayed increased binding to $KRAS^{G12V/I21F/H27R}$. To fully validate the functionality of the $KRAS^{G12V/I21F/H27R}$ mutant in cells, its effect on MAPK activation should be assessed. This can be done by evaluating phosphorylation levels of ERK (pERK) by immunoblot following expression of $KRAS^{G12V/I21F/H27R}$ versus $KRAS^{G12V}$, in the presence or absence of overexpressed RASSF5.

The aim of this M.Sc. project was to identify proteins involved in KRAS mediated activation of the Hippo pathway *via* RASSF1 or RASSF5, by mapping the interactomes of these three proteins by proximity biotinylation. We generated stable doxycycline-inducible U2OS cell lines expressing baits for BioID, either alone or jointly with a second overexpressed protein. To ensure that BioID will work reliably in our cell lines, we checked whether BirA*-tagged baits were capable of biotinylating known interactors. $KRAS^{G12V}$ and $KRAS^{G12V/I21F/H27R}$ were biotinylated when they were co-expressed with BirA*-RASSF5 although the expression of the exogenous proteins used in this experiment was not equal between conditions and therefore needs to be repeated. Nonetheless, this result validated that BirA*-tagged RASSF5 could interact with its binding partner $KRAS^{G12V}$. Similarly, exogenously expressed RASSF5 was biotinylated in the BioID lines expressing BirA*-tagged $KRAS^{G12V}$ or $KRAS^{G12V/I21F/H27R}$. Endogenous RAF1 was biotinylated in lines expressing BirA*-tagged $KRAS^{G12V}$ or $KRAS^{G12V/I21F/H27R}$ alone, or in combination with RASSF5. Interestingly, the band intensity pattern that we observed for RAF1 biotinylation (**Fig 12B**) was almost identical to the pattern of spectral abundance in the heat map row corresponding to RAF1 in the KRAS BioIDs (**Fig 15**). Both the BioID data and the immunoblot showed that the interaction between RAF1 and $KRAS^{G12V/I21F/H27R}$ was almost entirely lost upon overexpression of RASSF5, corroborating the functionality of this KRAS rewiring mutant. The interaction between RAF1 and $KRAS^{G12V}$ was not at all diminished when

RASSF5 was present, indicating that exogenous RASSF5 was not outcompeting endogenous RAF1 for binding to KRAS. It is worth mentioning that the anti-FLAG blot (**Fig 12B**) showed the opposite; the RAF1/KRAS^{G12V} interaction was diminished when RASSF5 was present. This discrepancy could be explained the following way: the peptide sequence recognized by the anti-RAF1 antibody used for this IP is near the RBD of RAF1, and thus binding of the antibody to RAF1 could be partially hindering binding of RAS. However, since the biotinylation of RAF1 occurs *in cellulo* prior to performing the IP, it wasn't affected by the binding of the antibody.

We successfully elucidated the interactome of KRAS, RASSF1, and RASSF5 in a total of eleven different conditions. Six of the conditions corresponded to the Hippo pathway in the inactive state, where KRAS or the RASSF proteins were overexpressed alone, with the remaining five conditions corresponding to a Hippo active state where both constitutively active KRAS and RASSF1 or RASSF5 were co-expressed. Analyzing the extensive data and comparing between active Hippo and inactive Hippo interactomes allowed us to make some interesting observations, draw several conclusions, and ask new questions.

The KRAS interaction with SNARE proteins

Soluble NSF attachment protein receptors (SNAREs) are a class of vesicle and membrane-associated proteins that facilitate the fusion between vesicles and target membranes, thus regulating release of vesicle cargo and transfer of membrane proteins to appropriate compartments (132). SNAP23, SNAP29 and VAMP3 are SNAREs implicated in the endosome to PM trafficking of KRAS. SNAP29 and VAMP3 are localized at endosomes, whereas SNAP23 localized at the PM and at endosomes to a lesser extent. Deletion of all three SNAREs leads to the accumulation of KRAS at recycling endosomes. Che *et al* have demonstrated by coimmunoprecipitation (co-IP) that SNAP23, SNAP29 and VAMP3 can associate with KRAS. Furthermore, using microscale thermophoresis, the authors calculated the binding affinities for the KRAS/SNAP23 and KRAS/SNAP29 interactions to be 117 nM and 178 nM respectively, whereas the interaction with VAMP3 is likely indirect (131).

Our KRAS BioID data showed an enrichment of these three SNARE proteins (as well as the SNARE protein VAMP2) in the conditions where RASSF5 was overexpressed. We hypothesized that expression of RASSF5 or activation of the Hippo pathway might be regulating KRAS vesicular trafficking and PM localization. Increased interaction between KRAS and the

SNARE proteins could be interpreted in two ways; (a) that there is an accumulation of KRAS in recycling endosomes and that KRAS is thus interacting more with these three endosomal proteins, (b) that there is an upregulation in expression of the three SNARE proteins, which are positive regulators of KRAS PM localization, and thus that there is an accumulation of KRAS at the PM. At first glance, explanation (a) is more appealing, given the tumor suppressive role of RASSF5. However, out of the three SNAREs, SNAP23 was the most significantly enriched in the presence of RASSF5 and it is primarily localized at the PM. Furthermore, RAB11B which was identified in the BioID of KRAS, was depleted when RASSF5 was expressed, despite its well characterized localization at recycling endosomes (133).

We confirmed that SNAP23 and VAMP3 are indeed proximal interactors of KRAS by performing a biotinylation-IP. However, we did not observe an increase in biotinylation of SNAP23 and VAMP3 when RASSF5 was co-expressed, although this experiment should be repeated while including $KRAS^{G12V/I21F/H27R}$. Furthermore, immunofluorescence experiments can be done to assess whether there is an accumulation of KRAS at recycling endosomes upon RASSF5 overexpression, using an endosomal marker such as ARF6.

The involvement of microtubules in Hippo signaling

RASSF1 binds and stabilizes microtubules (104). Unsurprisingly, the interactome of RASSF1 was highly enriched in microtubule-associated proteins. A number of MAPs, namely MAP1S and MAP1B, were also enriched in the interactomes of $RASSF1^{NCKL}$ and RASSF5, indicative of a potential role of RASSF5 at microtubules, despite its mostly nuclear localization. Moshkinova *et al* have previously observed endogenous RASSF5 localized at microtubules and at centrosomes in A549 lung adenocarcinoma cells, as well as in immortalized epithelial cells (134).

The *Drosophila* and human Hippo pathway interactomes, which were mapped by AP-MS, both contain microtubule-associated proteins (135,136). Namely, the *Drosophila* Hippo interactome shows an enrichment of MAPs involved in mitotic spindle reorganization (135). Hauri *et al* have mapped the human Hippo pathway interactome in HEK 293 cells, and they observed MST1/2 and RASSF1/3/5 in complex with MAP1S and MAP1B (136).

In our BioID datasets, the enrichment of most MAPs did not vary between interactomes, regardless of the expression of constitutively active KRAS. Interestingly however, α-tubulin and β-tubulin (TUBA1A, TUBA1C, TUBB2B, TUBB4B) were among the most highly enriched hits

in Hippo active conditions for RASSF1, RASSF5, and KRAS interactomes, adding further evidence of a link between microtubule dynamics and the Hippo pathway. Interestingly, an interaction between the RA domain RASSF5 and α/β-tubulin has been observed *in vitro* (137). Furthermore, RASSF5 can seemingly promote microtubule assembly *in vitro*, and this is impeded by active KRAS (137). A potential role of RASSF5 at microtubules *in vivo* should be investigated further, starting by validating the RASSF5/tubulin interaction by co-IP experiments.

Despite the proximity of RASSF1^{NCKL} and RASSF5 to MAPs and to tubulin, our BioID data does not contradict them having a nuclear localization, given that many nuclear proteins were among the BioID hits. In fact, the BioID datasets suggest that RASSF5 is in proximity to proteins in three different cellular localizations: the nucleus (enriched in the absence of KRAS^{G12V}), the plasma membrane (enriched in the presence of KRAS^{G12V}), and microtubules (α-tubulin and β-tubulin were enriched when KRAS^{G12V} or KRAS$^{G12V/I21F/H27R}$ were present).

The RASSF interaction with MST1/2

The MST1 and MST2 kinases, at the core of the Hippo pathway, were identified as preys in the interactomes of RASSF1, RASSF1^{NCKL} and RASSF5. The interaction of the RASSF proteins with MST1/2 was enriched in the absence of KRAS^{G12V} or KRAS$^{G12V/I21F/H27R}$. In other words, RASSF1/5 and MST1/2 interacted more when the Hippo pathway was inactive than when it was active. This finding aligns with the extensive *in vitro* data showing that RASSFs are inhibitors of MST1/2 kinase activity and agrees with a model whereby KRAS^{G12V} binds to its effector RASSF5 to promote release of MST1/2. However, exogenous expression of RASSF1/5 is required for KRAS-mediated activation of the Hippo pathway, since expression of KRAS^{G12V} alone does not result in activation. This suggests that the RASSF/MST interaction is nonetheless important for proper MST activation – for example, this interaction might be important for proper localization of the kinase at the site of Hippo pathway activation, or it might stabilize the MST protein, leading to increased expression, supporting the *reservoir model* (64).

Conversely, this reduced interaction between RASSF1/5 and MST1/2 during Hippo activation does not support the *membrane complex model* proposed in the literature whereby KRAS/RASSF5/MST form a complex at the PM (103). Furthermore, MST1 and MST2 were not identified in the interactome of KRAS with RASSF5. However, this model cannot be completely refuted. KRAS and RASSF5 might cooperate to recruit MST1/2 to the PM, where Hippo signaling

likely occurs. This would increase the local concentration of MST1/2, which would therefore promote MST1/2 homodimerization, release of RASSF5, and subsequent activation. Perhaps the KRAS/RASSF5/MST complex is very transient and only exists for a fraction of the time that the active MST1/2 dimers exist.

Given that binding between KRAS and RASSF1 is not required for Hippo activation, a third model is required to explain how KRAS mediates the release of the RASSF1/MST interaction. Proteins that might be involved in this indirect regulation are hits that displayed differential abundance between the RASSF1 alone and the RASSF1 with $KRAS^{G12V}$ interactomes. The proximal interaction between RASSF1 and DLG5 was markedly decreased when $KRAS^{G12V}$ was expressed. DLG5, which has been shown to inhibit the Hippo pathway by interacting with MST1/2, was also identified in the interactome of KRAS. Whether DLG5 is involved in KRAS regulation of the RASSF1/MST interaction should be investigated.

Conclusion

We successfully elucidated the interactome of KRAS, RASSF1, and RASSF5 in the context of Hippo signaling, while also demonstrating the merit of using a rewiring approach to study RAS signaling. We have generated an extensive database of proximal protein interactions to be further investigated by our lab and by the scientific community. Our BioID data provides intriguing evidence on how RASSF proteins regulate MST kinases *in vivo*, and validates a proximal interaction between KRAS and SNAP23 and VAMP3, supporting the findings of Che *et al*. However, we have only scratched the surface of our data; many interesting interactions remain to be validated, including interactions between RASSF5 and microtubules, RASSF1 and DLG5, and numerous others. While we demonstrated that the biotinylation-IP strategy is an effective initial validation step, the best validation strategy for protein interactions is to perform functional studies (113). The future direction of this project will include such studies, such as proliferation assays in KRAS-driven cancer cell lines.

The study of oncogenic RAS signaling in the last forty years has been crucial to our understanding of the molecular basis of oncogenesis. While it is important to keep studying the oncogenic MAPK and PI3K pathways downstream of RAS, it is equally vital to investigate how RAS signals to less studied effectors and pathways, particularly those with tumor suppressive functions like the Hippo pathway. There is a significant need for new treatments for RAS-driven

cancers, and the oncogene YAP presents a promising target in these highly malignant diseases. The development of therapies that inhibit YAP by activating the Hippo pathway is just an example of why gaining a better understanding of RAS signaling to this pathway is necessary.

References

1. Kolch W, Halasz M, Granovskaya M, Kholodenko BN. The dynamic control of signal transduction networks in cancer cells. Nature Reviews Cancer. 2015;15(9):515–27.
2. Simanshu DK, Nissley DV, McCormick F. RAS Proteins and Their Regulators in Human Disease. Cell. 2017 Jun;170(1):17–33.
3. Bos JL, Rehmann H, Wittinghofer A. GEFs and GAPs: Critical Elements in the Control of Small G Proteins. Cell. 2007 Jun;129(5):865–77.
4. Boriack-Sjodin PA, Margarit SM, Bar-Sagi D, Kuriyan J. The structural basis of the activation of Ras by Sos. Nature. 1998 Jul;394(6691):337–43.
5. Hunter JC, Manandhar A, Carrasco MA, Gurbani D, Gondi S, Westover KD. Biochemical and structural analysis of common cancer-associated KRAS mutations. Molecular Cancer Research. 2015;13(9):1325–35.
6. Scheffzek K, Ahmadian MR, Kabsch W, Wiesmüller L, Lautwein A, Schmitz F, et al. The Ras-RasGAP Complex: Structural Basis for GTPase Activation and Its Loss in Oncogenic Ras Mutants. Science. 1997 Jul;277(5324):333–8.
7. Colicelli J. Human RAS Superfamily Proteins and Related GTPases. Sci STKE. 2004 Sep 14;2004(250):1–31.
8. Wennerberg K, Rossman KL, Der CJ. The Ras superfamily at a glance. Journal of cell science. 2005 Mar;118(Pt 5):843–6.
9. Bernal Astrain G, Nikolova M, Smith MJ. Functional diversity in the RAS subfamily of small GTPases. Biochemical Society Transactions. 2022 Apr 29;50(2):921–33.
10. Ridley AJ. Rho GTPases and cell migration. Journal of Cell Science. 2001 Aug 1;114(15):2713–22.
11. Segev N. Ypt/Rab GTPases: Regulators of Protein Trafficking. Science STKE. 2001 Sep 18;2001(100):1–19.
12. Randazzo PA, Nie Z, Miura K, Hsu VW. Molecular Aspects of the Cellular Activities of ADP-Ribosylation Factors. Science STKE. 2000 Nov 1;2000(59):1–16.
13. Weis K. Regulating access to the genome: nucleocytoplasmic transport throughout the cell cycle. Cell. 2003 Feb 21;112(4):441–51.

14. Abankwa D, Gorfe AA, Inder K, Hancock JF. Ras membrane orientation and nanodomain localization generate isoform diversity. Proc Natl Acad Sci USA. 2010 Jan 19;107(3):1130–5.
15. Vogel A, Reuther G, Weise K, Triola G, Nikolaus J, Tan KT, et al. The Lipid Modifications of Ras that Sense Membrane Environments and Induce Local Enrichment. Angew Chem Int Ed. 2009 Nov 2;48(46):8784–7.
16. Weise K, Triola G, Brunsveld L, Waldmann H, Winter R. Influence of the Lipidation Motif on the Partitioning and Association of N-Ras in Model Membrane Subdomains. J Am Chem Soc. 2009 Feb 4;131(4):1557–64.
17. Reiss Y, Stradley SJ, Gierasch LM, Brown MS, Goldstein JL. Sequence requirement for peptide recognition by rat brain p21ras protein farnesyltransferase. Proc Natl Acad Sci USA. 1991 Feb;88(3):732–6.
18. Whyte DB, Kirschmeier P, Hockenberry TN, Nunez-Oliva I, James L, Catino JJ, et al. K- and N-Ras are geranylgeranylated in cells treated with farnesyl protein transferase inhibitors. Journal of Biological Chemistry. 1997;272(22):14459–64.
19. Kirsten WH, Mayer LA. Malignant Lymphomas of Extrathymic Origin Induced in Rats by Murine Erythroblastosis Virus2. JNCI: Journal of the National Cancer Institute. 1969 Sep;43(3):735–46.
20. Harvey JJ. An unidentified virus which causes the rapid production of tumours in mice. Nature. 1964 Dec 12;204:1104–5.
21. Moore AR, Rosenberg SC, McCormick F, Malek S. RAS-targeted therapies: is the undruggable drugged? Nat Rev Drug Discov. 2020 Aug 15;19(8):533–52.
22. Lemmon MA, Schlessinger J. Cell Signaling by Receptor Tyrosine Kinases. Cell. 2010 Jun;141(7):1117–34.
23. Nakhaeizadeh H, Amin E, Nakhaei-Rad S, Dvorsky R, Ahmadian MR. The RAS-effector interface: Isoform-specific differences in the effector binding regions. PLoS ONE. 2016;11(12):e0167145–e0167145.
24. Singh S, Smith MJ. RAS GTPase signalling to alternative effector pathways. Biochemical Society Transactions. 2020;48(5):2241–52.
25. Vojtek AB, Hollenberg SM, Cooper JA. Mammalian Ras interacts directly with the serine/threonine kinase raf. Cell. 1993 Jul;74(1):205–14.

26. Warne PH, Vician PR, Downward J. Direct interaction of Ras and the amino-terminal region of Raf-1 in vitro. Nature. 1993 Jul;364(6435):352–5.
27. Zhang X feng, Settleman J, Kyrlakis JM, Takeuchi-Suzuki E, Elledge SJ, Marshallt MS, et al. Normal and oncogenic p21ras proteins bind to the amino-terminal regulatory domain of c-Raf-1. Nature. 1993 Jul 12;364(6435):308–13.
28. Freeman AK, Ritt DA, Morrison DK. The importance of Raf dimerization in cell signaling. Small GTPases. 2013 Jul;4(3):180–5.
29. Yoon S, Seger R. The extracellular signal-regulated kinase: Multiple substrates regulate diverse cellular functions. Growth Factors. 2006 Jan;24(1):21–44.
30. Rapp UR, Goldsborough MD, Mark GE, Bonner TI, Groffen J, Reynolds FH, et al. Structure and biological activity of v-raf, a unique oncogene transduced by a retrovirus. Proc Natl Acad Sci USA. 1983 Jul;80(14):4218–22.
31. White MA, Nicolette C, Minden A, Polverino A, Aelst LV, Karin M, et al. Multiple ras functions can contribute to mammalian cell transformation. Cell. 1995 Feb;80(4):533–41.
32. Khwaja A. Matrix adhesion and Ras transformation both activate a phosphoinositide 3-OH kinase and protein kinase B/Akt cellular survival pathway. The EMBO Journal. 1997 May 15;16(10):2783–93.
33. Rodriguez-Viciana P, Warne PH, Khwaja A, Marte BM, Pappin D, Das P, et al. Role of Phosphoinositide 3-OH Kinase in Cell Transformation and Control of the Actin Cytoskeleton by Ras. Cell. 1997 May;89(3):457–67.
34. Rodriguez-Viciana P, Warne PH, Dhandt R, Vanhaesebroeckt B, Goutt I, Fry MJ, et al. Phosphatidylinositol-3-OH kinase as a direct target of Ras. Nature. 1994 Aug;370(6490):527–32.
35. Rodriguez-Viciana P, Warne PH, Vanhaesebroeck B, Waterfield MD, Downward J. Activation of phosphoinositide 3-kinase by interaction with Ras and by point mutation. The EMBO Journal. 1996 May;15(10):2442–51.
36. Castellano E, Downward J. Ras interaction with PI3K: More than just another effector pathway. Genes and Cancer. 2011;2(3):261–74.
37. Neel NF, Martin TD, Stratford JK, Zand TP, Reiner DJ, Der CJ. The RalGEF-ral effector signaling network: The road less traveled for anti-ras drug discovery. Genes and Cancer. 2011;2(3):275–87.

38. Yan C, Theodorescu D. RAL GTpases: Biology and potential as therapeutic targets in cancer. Pharmacological Reviews. 2018;70(1):1–11.
39. Rodriguez-Viciana P, McCormick F. RalGDS comes of age. Cancer Cell. 2005;
40. Goudreault M, Gagné V, Jo CH, Singh S, Killoran RC, Gingras AC, et al. Afadin couples RAS GTPases to the polarity rheostat Scribble. Nat Commun. 2022 Aug 5;13(1):4562.
41. Bunney TD, Harris R, Josephs MB, Roe SM, Sorli SC, Paterson HF, et al. Structural and Mechanistic Insights into Ras Association Domains of Phospholipase C Epsilon. 2006;495–507.
42. Wang Y, Waldron RT, Dhaka A, Patel A, Riley MM, Rozengurt E, et al. The RAS Effector RIN1 Directly Competes with RAF and Is Regulated by 14-3-3 Proteins. Mol Cell Biol. 2002 Feb;22(3):916–26.
43. Stephen AG, Esposito D, Bagni RK, McCormick F. Dragging Ras Back in the Ring. Cancer Cell. 2014 Mar;25(3):272–81.
44. von Lintig FC, Dreilinger AD, Varki NM, Wallace AM, Casteel DE, Boss GR. Ras activation in human breast cancer. Breast Cancer Res Treat. 2000 Jul;62(1):51–62.
45. Bustelo XR, Crespo P, Fernández-Pisonero I, Rodríguez-Fdez S. RAS GTPase-dependent pathways in developmental diseases: old guys, new lads, and current challenges. Current Opinion in Cell Biology. 2018;55:42–51.
46. Pylayeva-Gupta Y, Grabocka E, Bar-Sagi D. RAS oncogenes: Weaving a tumorigenic web. Nature Reviews Cancer. 2011;11(11):761–74.
47. Zhang SS, Nagasaka M. Spotlight on Sotorasib (AMG 510) for KRASG12C Positive Non-Small Cell Lung Cancer. LCTT. 2021 Oct;Volume 12:115–22.
48. Ostrem JM, Peters U, Sos ML, Wells JA, Shokat KM. K-Ras(G12C) inhibitors allosterically control GTP affinity and effector interactions. Nature. 2013 Nov;503(7477):548–51.
49. Wu S, Huang J, Dong J, Pan D. hippo Encodes a Ste-20 Family Protein Kinase that Restricts Cell Proliferation and Promotes Apoptosis in Conjunction with salvador and warts. Cell. 2003 Aug;114(4):445–56.
50. Avruch J, Zhou D, Fitamant J, Bardeesy N, Mou F, Barrufet LR. Protein kinases of the Hippo pathway: Regulation and substrates. Seminars in Cell & Developmental Biology. 2012 Sep;23(7):770–84.

51. Pantalacci S, Tapon N, Léopold P. The Salvador partner Hippo promotes apoptosis and cell-cycle exit in Drosophila. Nat Cell Biol. 2003 Oct;5(10):921–7.
52. Dong J, Feldmann G, Huang J, Wu S, Zhang N, Comerford SA, et al. Elucidation of a Universal Size-Control Mechanism in Drosophila and Mammals. Cell. 2007 Sep;130(6):1120–33.
53. Harvey KF, Zhang X, Thomas DM. The Hippo pathway and human cancer. Nat Rev Cancer. 2013 Apr;13(4):246–57.
54. Zhao B, Wei X, Li W, Udan RS, Yang Q, Kim J, et al. Inactivation of YAP oncoprotein by the Hippo pathway is involved in cell contact inhibition and tissue growth control. Genes Dev. 2007 Nov 1;21(21):2747–61.
55. Lei QY, Zhang H, Zhao B, Zha ZY, Bai F, Pei XH, et al. TAZ Promotes Cell Proliferation and Epithelial-Mesenchymal Transition and Is Inhibited by the Hippo Pathway. Mol Cell Biol. 2008 Apr;28(7):2426–36.
56. Hong W, Guan KL. The YAP and TAZ transcription co-activators: Key downstream effectors of the mammalian Hippo pathway. Seminars in Cell & Developmental Biology. 2012 Sep;23(7):785–93.
57. Hergovich A, Schmitz D, Hemmings BA. The human tumour suppressor LATS1 is activated by human MOB1 at the membrane. Biochemical and Biophysical Research Communications. 2006 Jun;345(1):50–8.
58. Ni L, Zheng Y, Hara M, Pan D, Luo X. Structural basis for Mob1-dependent activation of the core Mst–Lats kinase cascade in Hippo signaling. Genes Dev. 2015 Jul 1;29(13):1416–31.
59. Steinhardt AA, Gayyed MF, Klein AP, Dong J, Maitra A, Pan D, et al. Expression of Yes-associated protein in common solid tumors. Human Pathology. 2008 Nov;39(11):1582–9.
60. Zender L, Spector MS, Xue W, Flemming P, Cordon-Cardo C, Silke J, et al. Identification and Validation of Oncogenes in Liver Cancer Using an Integrative Oncogenomic Approach. Cell. 2006 Jun;125(7):1253–67.
61. Kapoor A, Yao W, Ying H, Hua S, Liewen A, Wang Q, et al. Yap1 Activation Enables Bypass of Oncogenic Kras Addiction in Pancreatic Cancer. Cell. 2014 Jul;158(1):185–97.

62. Shao DD, Xue W, Krall EB, Bhutkar A, Piccioni F, Wang X, et al. KRAS and YAP1 converge to regulate EMT and tumor survival. Cell. 2014;158(1):171–84.
63. Singh K, Pruski MA, Polireddy K, Jones NC, Chen Q, Yao J, et al. Mst1/2 kinases restrain transformation in a novel transgenic model of Ras driven non-small cell lung cancer. Oncogene. 2020 Jan 30;39(5):1152–64.
64. Praskova M, Khoklatchev A, Ortiz-Vega S, Avruch J. Regulation of the MST1 kinase by autophosphorylation, by the growth inhibitory proteins, RASSF1 and NORE1, and by Ras. Biochemical Journal. 2004;381(2):453–62.
65. Ni L, Li S, Yu J, Min J, Brautigam CA, Tomchick DR, et al. Structural Basis for Autoactivation of Human Mst2 Kinase and Its Regulation by RASSF5. Structure. 2013 Oct;21(10):1757–68.
66. Tran T, Mitra J, Ha T, Kavran JM. Increasing kinase domain proximity promotes MST2 autophosphorylation during Hippo signaling. Journal of Biological Chemistry. 2020 Nov;295(47):16166–79.
67. Koehler TJ, Tran T, Weingartner KA, Kavran JM. Kinetic Regulation of the Mammalian Sterile 20-like Kinase 2 (MST2). Biochemistry. 2022 Aug 16;61(16):1683–93.
68. Cordenonsi M, Zanconato F, Azzolin L, Forcato M, Rosato A, Frasson C, et al. The Hippo Transducer TAZ Confers Cancer Stem Cell-Related Traits on Breast Cancer Cells. Cell. 2011 Nov;147(4):759–72.
69. Overholtzer M, Zhang J, Smolen GA, Muir B, Li W, Sgroi DC, et al. Transforming properties of *YAP* , a candidate oncogene on the chromosome 11q22 amplicon. Proc Natl Acad Sci USA. 2006 Aug 15;103(33):12405–10.
70. Hanahan D, Weinberg RA. Hallmarks of Cancer: The Next Generation. Cell. 2011 Mar;144(5):646–74.
71. Lefort S, Tan S, Balani S, Rafn B, Pellacani D, Hirst M, et al. Initiation of human mammary cell tumorigenesis by mutant KRAS requires YAP inactivation. Oncogene. 2020 Feb 27;39(9):1957–68.
72. Slemmons KK, Yeung C, Baumgart JT, Juarez JOM, McCalla A, Helman LJ. Targeting Hippo-Dependent and Hippo-Independent YAP1 Signaling for the Treatment of Childhood Rhabdomyosarcoma. Cancer research. 2020;80(14):3046–56.

73. Coggins GE, Farrel A, Rathi KS, Hayes CM, Scolaro L, Rokita JL, et al. YAP1 mediates resistance to MEK1/2 inhibition in neuroblastomas with hyperactivated Ras signaling. Cancer Research. 2019;79(24):6204–14.
74. Dupont S, Morsut L, Aragona M, Enzo E, Giulitti S, Cordenonsi M, et al. Role of YAP/TAZ in mechanotransduction. Nature. 2011 Jun;474(7350):179–83.
75. Wada KI, Itoga K, Okano T, Yonemura S, Sasaki H. Hippo pathway regulation by cell morphology and stress fibers. Development. 2011 Sep 15;138(18):3907–14.
76. Fernández BG, Gaspar P, Brás-Pereira C, Jezowska B, Rebelo SR, Janody F. Actin-Capping Protein and the Hippo pathway regulate F-actin and tissue growth in *Drosophila*. Development. 2011 Jun 1;138(11):2337–46.
77. Sansores-Garcia L, Bossuyt W, Wada KI, Yonemura S, Tao C, Sasaki H, et al. Modulating F-actin organization induces organ growth by affecting the Hippo pathway. The EMBO Journal. 2011 Jun 15;30(12):2325–35.
78. Schroeder MC, Halder G. Regulation of the Hippo pathway by cell architecture and mechanical signals. Seminars in Cell & Developmental Biology. 2012 Sep;23(7):803–11.
79. Zhao B, Li L, Wang L, Wang CY, Yu J, Guan KL. Cell detachment activates the Hippo pathway via cytoskeleton reorganization to induce anoikis. Genes Dev. 2012 Jan 1;26(1):54–68.
80. Rausch V, Hansen CG. The Hippo Pathway, YAP/TAZ, and the Plasma Membrane. Trends in Cell Biology. 2020 Jan;30(1):32–48.
81. Piccolo S, Dupont S, Cordenonsi M. The Biology of YAP/TAZ: Hippo Signaling and Beyond. Physiological Reviews. 2014 Oct;94(4):1287–312.
82. Kwan J, Sczaniecka A, Heidary Arash E, Nguyen L, Chen CC, Ratkovic S, et al. DLG5 connects cell polarity and Hippo signaling protein networks by linking PAR-1 with MST1/2. Genes Dev. 2016 Dec 15;30(24):2696–709.
83. Grusche FA, Richardson HE, Harvey KF. Upstream Regulation of the Hippo Size Control Pathway. Current Biology. 2010 Jul;20(13):R574–82.
84. Yin F, Yu J, Zheng Y, Chen Q, Zhang N, Pan D. Spatial Organization of Hippo Signaling at the Plasma Membrane Mediated by the Tumor Suppressor Merlin/NF2. Cell. 2013 Sep;154(6):1342–55.

85. Li Y, Zhou H, Li F, Chan SW, Lin Z, Wei Z, et al. Angiomotin binding-induced activation of Merlin/NF2 in the Hippo pathway. Cell Res. 2015 Jul;25(7):801–17.
86. Yu FX, Zhao B, Panupinthu N, Jewell JL, Lian I, Wang LH, et al. Regulation of the Hippo-YAP Pathway by G-Protein-Coupled Receptor Signaling. Cell. 2012 Aug;150(4):780–91.
87. Stieglitz B, Bee C, Schwarz D, Yildiz Ö, Moshnikova A, Khokhlatchev A, et al. Novel type of Ras effector interaction established between tumour suppressor NORE1A and Ras switch II. The EMBO Journal. 2008 Jul;27(14):1995–2005.
88. Dhanaraman T, Singh S, Killoran RC, Singh A, Xu X, Shifman JM, et al. RASSF effectors couple diverse RAS subfamily GTPases to the Hippo pathway. Science Signaling. 2020 Oct;13(653):eabb4778–eabb4778.
89. Dammann R, Li C, Yoon JH, Chin PL, Bates S, Pfeifer GP. Epigenetic inactivation of a RAS association domain family protein from the lung tumour suppressor locus 3p21.3. Nat Genet. 2000 Jul;25(3):315–9.
90. Burbee DG, Forgacs E, Zochbauer-Muller S, Shivakumar L, Fong K, Gao B, et al. Epigenetic Inactivation of RASSF1A in Lung and Breast Cancers and Malignant Phenotype Suppression. JNCI Journal of the National Cancer Institute. 2001 May 2;93(9):691–9.
91. Agathanggelou A, Honorio S, Macartney DP, Martinez A, Dallol A, Rader J, et al. Methylation associated inactivation of RASSF1A from region 3p21.3 in lung, breast and ovarian tumours. Oncogene. 2001 Mar 22;20(12):1509–18.
92. Liu L, Yoon JH, Dammann R, Pfeifer GP. Frequent hypermethylation of the RASSF1A gene in prostate cancer. Oncogene. 2002 Oct 3;21(44):6835–40.
93. Tommasi S, Dammann R, Zhang Z, Wang Y, Liu L, Tsark WM, et al. Tumor Susceptibility of *Rassf1a* Knockout Mice. Cancer Research. 2005 Jan 1;65(1):92–8.
94. Hesson L, Dallol A, Minna JD, Maher ER, Latif F. NORE1A, a homologue of RASSF1A tumour suppressor gene is inactivated in human cancers. Oncogene. 2003 Feb 13;22(6):947–54.
95. Chen J, Lui WO, Vos MD, Clark GJ, Takahashi M, Schoumans J, et al. The t(1;3) breakpoint-spanning genes LSAMP and NORE1 are involved in clear cell renal cell carcinomas. Cancer Cell. 2003 Nov;4(5):405–13.

96. Aoyama Y, Avruch J, Zhang XF. Nore1 inhibits tumor cell growth independent of Ras or the MST1/2 kinases. Oncogene. 2004;23(19):3426–33.
97. Park J, Kang SI, Lee SY, Zhang XF, Kim MS, Beers LF, et al. Tumor suppressor Ras association domain family 5 (RASSF5/NORE1) mediates death receptor ligand-induced apoptosis. Journal of Biological Chemistry. 2010;285(45):35029–38.
98. Baksh S, Tommasi S, Fenton S, Yu VC, Martins LM, Pfeifer GP, et al. The tumor suppressor RASSF1A and MAP-1 link death receptor signaling to bax conformational change and cell death. Molecular Cell. 2005;18(6):637–50.
99. Matallanas D, Romano D, Yee K, Meissl K, Kucerova L, Piazzolla D, et al. RASSF1A Elicits Apoptosis through an MST2 Pathway Directing Proapoptotic Transcription by the p73 Tumor Suppressor Protein. Molecular Cell. 2007 Sep;27(6):962–75.
100. Foley CJ, Freedman H, Choo SL, Onyskiw C, Fu NY, Yu VC, et al. Dynamics of RASSF1A/MOAP-1 Association with Death Receptors. Mol Cell Biol. 2008 Jul 15;28(14):4520–35.
101. Vichalkovski A, Gresko E, Cornils H, Hergovich A, Schmitz D, Hemmings BA. NDR Kinase Is Activated by RASSF1A/MST1 in Response to Fas Receptor Stimulation and Promotes Apoptosis. Current Biology. 2008 Dec;18(23):1889–95.
102. Oh HJ, Lee KK, Song SJ, Jin MS, Song MS, Lee JH, et al. Role of the tumor suppressor RASSF1A in Mst1-mediated apoptosis. Cancer Research. 2006;66(5):2562–9.
103. Khokhlatchev A, Rabizadeh S, Xavier R, Nedwidek M, Chen T, Zhang X feng, et al. Identification of a Novel Ras-Regulated Proapoptotic Pathway. Current Biology. 2002 Feb;12(4):253–65.
104. Liu L, Tommasi S, Lee DH, Dammann R, Pfeifer GP. Control of microtubule stability by the RASSF1A tumor suppressor. Oncogene. 2003 Nov 6;22(50):8125–36.
105. Ortiz-Vega S, Khokhlatchev A, Nedwidek M, Zhang XFF, Dammann R, Pfeifer GP, et al. The putative tumor suppressor RASSF1A homodimerizes and heterodimerizes with the Ras-GTP binding protein Nore1. Oncogene. 2002;21(9):1381–90.
106. Hwang E, Ryu KS, Pääkkönen K, Güntert P, Cheong HK, Lim DS, et al. Structural insight into dimeric interaction of the SARAH domains from Mst1 and RASSF family proteins in the apoptosis pathway. Proceedings of the National Academy of Sciences of the United States of America. 2007;104(22):9236–41.

107. Bitra A, Sistla S, Mariam J, Malvi H, Anand R. Rassf Proteins as Modulators of Mst1 Kinase Activity. Sci Rep. 2017 Jul;7(1):45020.
108. White MA, Vale T, Camonis JH, Schaefer E, Wigler MH. A role for the Ral guanine nucleotide dissociation stimulator in mediating Ras-induced transformation. Journal of Biological Chemistry. 1996;271(28):16439–42.
109. Khosravi-Far R, White MA, Westwick JK, Solski PA, Chrzanowska-Wodnicka M, Van Aelst L, et al. Oncogenic Ras activation of Raf/mitogen-activated protein kinase-independent pathways is sufficient to cause tumorigenic transformation. Mol Cell Biol. 1996 Jul;16(7):3923–33.
110. Joneson T, White MA, Wigler MH, Bar-Sagi D. Stimulation of Membrane Ruffling and MAP Kinase Activation by Distinct Effectors of RAS. Science. 1996 Feb 9;271(5250):810–2.
111. Rodriguez-Viciana P. Phosphatidylinositol 3′ kinase : One of the effectors of Ras. Philosophical Transactions of the Royal Society B: Biological Sciences. 1996;
112. Roux KJ, Kim DI, Raida M, Burke B. A promiscuous biotin ligase fusion protein identifies proximal and interacting proteins in mammalian cells. Journal of Cell Biology. 2012 Mar 19;196(6):801–10.
113. Gingras AC, Abe KT, Raught B. Getting to know the neighborhood: using proximity-dependent biotinylation to characterize protein complexes and map organelles. Current Opinion in Chemical Biology. 2019 Feb;48:44–54.
114. Youn JY, Dyakov BJA, Zhang J, Knight JDR, Vernon RM, Forman-Kay JD, et al. Properties of Stress Granule and P-Body Proteomes. Molecular Cell. 2019;76(2):286–94.
115. Gupta GD, Coyaud É, Gonçalves J, Mojarad BA, Liu Y, Wu Q, et al. A Dynamic Protein Interaction Landscape of the Human Centrosome-Cilium Interface. Cell. 2015 Dec;163(6):1484–99.
116. Bersuker K, Peterson CWH, To M, Sahl SJ, Savikhin V, Grossman EA, et al. A Proximity Labeling Strategy Provides Insights into the Composition and Dynamics of Lipid Droplet Proteomes. Developmental Cell. 2018 Jan;44(1):97-112.e7.
117. Go CD, Knight JDR, Rajasekharan A, Rathod B, Hesketh GG, Abe KT, et al. A proximity-dependent biotinylation map of a human cell. Nature. 2021 Jul 1;595(7865):120–4.

118. He L, Diedrich J, Chu YY, Yates JR. Extracting Accurate Precursor Information for Tandem Mass Spectra by RawConverter. Anal Chem. 2015 Nov 17;87(22):11361–7.
119. Craig R, Beavis RC. TANDEM: matching proteins with tandem mass spectra. Bioinformatics. 2004 Jun 12;20(9):1466–7.
120. Liu G, Zhang J, Choi H, Lambert J, Srikumar T, Larsen B, et al. Using ProHits to Store, Annotate, and Analyze Affinity Purification–Mass Spectrometry (AP-MS) Data. Current Protocols in Bioinformatics. 2012 Sep;39(1):1–8.
121. Zybailov B, Mosley AL, Sardiu ME, Coleman MK, Florens L, Washburn MP. Statistical Analysis of Membrane Proteome Expression Changes in *Saccharomyces c erevisiae*. J Proteome Res. 2006 Sep 1;5(9):2339–47.
122. Choi H, Larsen B, Lin ZY, Breitkreutz A, Mellacheruvu D, Fermin D, et al. SAINT: probabilistic scoring of affinity purification–mass spectrometry data. Nat Methods. 2011 Jan;8(1):70–3.
123. Samavarchi-Tehrani P, Abdouni H, Samson R, Gingras AC. A Versatile Lentiviral Delivery Toolkit for Proximity-dependent Biotinylation in Diverse Cell Types. Molecular & Cellular Proteomics. 2018;17(11):2256–69.
124. Lim S, Yang MH, Park JH, Nojima T, Hashimoto H, Unni KK, et al. Inactivation of the RASSF1A in osteosarcoma. Oncol Rep. 2003 Aug;10(4):897–901.
125. Wang WG, Chen SJ, He JS, Li JS, Zang XF. The tumor suppressive role of RASSF1A in osteosarcoma through the Wnt signaling pathway. Tumor Biol. 2016 Jul;37(7):8869–77.
126. Zhou XH, Yang CQ, Zhang CL, Gao Y, Yuan HB, Wang C. RASSF5 inhibits growth and invasion and induces apoptosis in osteosarcoma cells through activation of MST1/LATS1 signaling. Oncology Reports. 2014 Oct;32(4):1505–12.
127. Adhikari H, Counter CM. Interrogating the protein interactomes of RAS isoforms identifies PIP5K1A as a KRAS-specific vulnerability. Nature Communications. 2018;9(1).
128. Kovalski JR, Bhaduri A, Zehnder AM, Neela PH, Che Y, Wozniak GG, et al. The Functional Proximal Proteome of Oncogenic Ras Includes mTORC2. Molecular Cell. 2019;73(4):830-844.e12.
129. Oughtred R, Stark C, Breitkreutz BJ, Rust J, Boucher L, Chang C, et al. The BioGRID interaction database: 2019 update. Nucleic Acids Research. 2019 Jan;47(D1):D529–41.

130. Roux KJ, Kim DI, Burke B, May DG. BioID: A Screen for Protein-Protein Interactions. Current Protocols in Protein Science. 2018 Jan;91(1).
131. Che Y, Siprashvili Z, Kovalski JR, Jiang T, Wozniak G, Elcavage L, et al. KRAS regulation by small non-coding RNAs and SNARE proteins. Nat Commun. 2019 Dec;10(1):5118.
132. Yoon TY, Munson M. SNARE complex assembly and disassembly. Current Biology. 2018 Apr;28(8):R397–401.
133. Takahashi S, Kubo K, Waguri S, Yabashi A, Shin HW, Katoh Y, et al. Rab11 regulates exocytosis of recycling vesicles at the plasma membrane. Journal of Cell Science. 2012 Jan 1;jcs.102913.
134. Moshnikova A, Frye J, Shay JW, Minna JD, Khokhlatchev AV. The Growth and Tumor Suppressor NORE1A Is a Cytoskeletal Protein That Suppresses Growth by Inhibition of the ERK Pathway. Journal of Biological Chemistry. 2006 Mar;281(12):8143–52.
135. Kwon Y, Vinayagam A, Sun X, Dephoure N, Gygi SP, Hong P, et al. The Hippo Signaling Pathway Interactome. Science. 2013 Nov 8;342(6159):737–40.
136. Hauri S, Wepf A, Drogen A, Varjosalo M, Tapon N, Aebersold R, et al. Interaction proteome of human Hippo signaling: modular control of the co-activator YAP1. Mol Syst Biol. 2013 Jan;9(1):713.
137. Bee C, Moshnikova A, Mellor CD, Molloy JE, Koryakina Y, Stieglitz B, et al. Growth and Tumor Suppressor NORE1A Is a Regulatory Node between Ras Signaling and Microtubule Nucleation. Journal of Biological Chemistry. 2010 May;285(21):16258–66.